We are IntechOpen,
the world's leading publisher of
Open Access books
Built by scientists, for scientists

4,800
Open access books available

122,000
International authors and editors

135M
Downloads

Our authors are among the

154
Countries delivered to

TOP 1%
most cited scientists

12.2%
Contributors from top 500 universities

BOOK CITATION INDEX
CLARIVATE ANALYTICS
INDEXED

WEB OF SCIENCE™

Selection of our books indexed in the Book Citation Index
in Web of Science™ Core Collection (BKCI)

Interested in publishing with us?
Contact book.department@intechopen.com

Natural vs Anthropogenic Background Aerosol Contribution to the Radiation Budget over Indian Thar Desert

Sanat Kumar Das

1. Introduction

In recent times, atmospheric aerosols are receiving increasing attention as they directly affect the Earth's radiation balance by altering incoming shortwave solar radiation that can cause positive (heating) or negative (cooling) radiative forcing depending on their scattering and absorption properties, the reflectivity of the underlying surface [10, 24] and the position of aerosols with respect to the global cloud coverage [8, 88]. Aerosols also affect the outgoing longwave radiation by absorption, emission and scattering. Presently, effects of radiative forcing of atmospheric aerosols on climate is a subject of great concern to atmospheric researchers. An accurate quantification of the aerosol direct radiative forcing is critical for the interpretation of existing climate records and also for the projection of future climate change [11, 47]. Significant amount of atmospheric radiative forcing causes high atmospheric heating due to strong absorption of solar radiation which can change the regional atmospheric stability and may alter the large scale circulation and the hydrological cycle, enough so, apparently, to account for observed temperature and precipitation changes in China and India [1, 46, 62, 70]. Therefore, the effect of aerosols on the radiation budget in terms of radiative forcing calculations is challenging and demanding, especially on the regional scale for the exclusive understanding of climate change.

The uncertainties involved in the climate models are mainly due to optical properties of aerosols on the regional scale, specially underestimated absorption of solar radiation by aerosols, both, naturally and anthropogenically produced [34], their residence time [57, 58], etc, which arise mostly due to lack of observations. Black carbon (BC) or soot and dust aerosols are playing the leading role in aerosol interaction with the solar radiation due to their strong absorption properties. BC comes into the atmosphere during combustion of fossil fuels, principally, diesel and coal, and from biomass burning. BC demands large attention due to its strong absorption of incoming solar radiation and produces positive radiative forcing which is sometimes comparable to the forcing of the green-house gas methane [31].

Therefore, underestimation of BC can introduce large uncertainty in the climate models. On the other hand, dust, mainly coming from arid regions, is generally known for scattering of solar radiation. However, dust also has a strong absorption in the UV and infrared regimes and therefore, can influence radiative forcing not only in the shortwave region but also in the longwave region. Hence, the study of dust aerosols is equally important. In addition, long-range transported dust aerosols can enhance the atmospheric radiative forcing in the presence of soot aerosols [14, 54].

South-East Asia, with its fast growing urbanization and industrialization, is one of the major hot-spot regions on the global aerosol map. A study of historical records from different locations on the globe reported an increasing trend of BC emissions in South and Central Asia [6]. In addition, dust aerosols are also transported from the Middle-East region to over South-East Asia. A mixture of locally produced anthropogenic aerosols with natural aerosols like mineral dust and seasalt, reported over this hot spot region [42, 60–62] aids in the warming of the atmosphere. There were several campaigns of ship-, land- and air-borne measurements over Indian subcontinent and surrounding marine regions to investigate the regional effects of anthropogenic aerosols [32, 48, 75, etc.]. In-situ measurements during the Indian Ocean Experiment (INDOEX) and several campaigns under Indian Space Research Organisation – Geosphere Biosphere Programme (ISRO–GBP) found that the sources of the anthropogenic aerosols are biomass burning and fossil-fuel combustions [33, 61]. The second phase of the ISRO-GBP land campaign during winter conducted in the Indo-Gangetic Plain (IGP), a hot-spot region over India, reported significant anthropogenic aerosol loading in the atmosphere coming from industries and vehicular emissions [15, 18, 50]. Satellite-based observations suggested that significant amount of dust is also transported over IGP from Thar Desert located in western India during premonsoon (March to May) [16, 17, 54]. This transported dust helps to sustain the hot-spot over IGP maintaining the large background aerosol loading. Majority of the earlier research works focused on aerosol contribution, either locally produced anthropogenic aerosols or transported natural dust, to regional climate change over this hot-spot region. However, uncertainties in those results are found to be relatively large, especially in studies on transported dust, as the dust becomes aged by externally and internally mixing with locally produced pollutants.

This chapter investigates and quantifies the natural and anthropogenic contribution of background aerosols over western India where both the source regions, Thar Desert, source of natural dust, and IGP, hot spot region of anthropogenic aerosols, are present. The contributions of both types of aerosols are estimated for the years 2006 and 2007 from ground-based and satellite measurements of aerosol optical and physical properties. Ground-based observations have been conducted at Mt. Abu (24.65°N, 72.78°E, 1.7 km asl), the highest location in Aravalli mountains in western India. The main advantage of the location is its proximity to both, Thar Desert and IGP. Also, due to the high altitude, the observation site is less affected by the boundary layer aerosols. The hill-top background aerosols are significantly influenced by wind that carries aerosols from either Thar Desert or IGP and show strong seasonal variation. Therefore, the site becomes a unique location for the investigation of both, natural and anthropogenic aerosols. The present study investigates the seasonal variation of aerosol properties at Mt. Abu and estimates the contribution of both aerosols on the radiation budget during the four seasons – winter (Dec-Feb), premonsoon (Mar-May), monsoon (Jun-Aug), and postmonsoon (Sep-Nov).

2. Datasets

2.1. Ground-based instruments

2.1.1. Microtops

Aerosol Optical Depth (AOD) was measured using a hand-held Microtops II (Solar Light Co., Inc., USA) [49] at every five minutes interval during daytime from 0730 to 1600 hours. This instrument can measure AOD at five different wavelengths centered at 0.380, 0.440, 0.500, 0.675, 0.870 μm simultaneously. Another Mictotops II was used to measure AOD at 1.020 μm associated with ozone and columnar water vapor . Both Microtops were regularly calibrated, once in a month, and all calibrated constants were obtained from Langley's plot analysis [30]. There is only 1% variation in the calibration constant since 2002. The absolute uncertainty of measured AOD is not more than 0.03 at all wavelengths [33].

2.1.2. QCM

Aerosol Mass Concentration was measured using a 10-stage Quartz Crystal Microbalance (QCM) cascade impactor (model PC-2, California Measurements Inc., USA) and the aerosol size distribution at the ground level was determined. Aerosols were collected in 10 stages of the impactor with cut-off radii at 12.5, 6.25, 3.2, 1.6, 0.8, 0.4, 0.2, 0.1, 0.05 and 0.025 μm from stage 1 to 10 respectively. The air flow rate through the impactor was kept at 240 ml/min and the typical sampling period was 300 sec for each measurement. The QCM was operated from the terrace of the observatory building at a height of about 6m. The air inlet was installed vertically to minimize the loss of aerosol particles within the inlet tube. The relative temperature change of the crystals during each sampling period of 5 minute is too small and can be neglected. Uncertainties involved in the QCM measurements are mainly due to variations in RH [15, 33, 59]. In an earlier study, the QCM was operated simultaneously with an Anderson impactor to investigate the measurement accuracy of each stage and it was observed that measurement error is always less than 15% [33].

2.1.3. Aethalomater

Absorbing aerosol mass concentrations at seven different wavelengths (centered at 0.37, 0.47, 0.52, 0.59, 0.66, 0.88 and 0.95 μm) were obtained using a multichannel Aethalometer (model AE-42) manufactured by Magee Scientific, USA [21]. The flow rate of ambient air was maintained at 3.0 l.min^{-1} and the data was stored in the memory disk at a time interval of two minutes during the measurement period. BC mass concentration is estimated by detecting the light transmitted through the particle deposited sample spot and particle free reference spot on the filter as follows [5, 89]

$$BC = -\frac{A\,100\ln\left(\frac{I_2}{I_1}\right)}{kQ\Delta t} \tag{1}$$

where I_1 and I_2 are the ratios of light intensities of the sample beam to the reference beam before and after particle sampling at time interval Δt, Q is the volume flow rate of the ambient air through the filter, A is the area of the sample spot and k is the absorption coefficient. The real-time BC mass concentration is considered at 0.88 μm wavelength channel because the spectral response of elemental carbon particles has a peak near this wavelength [5]. The manufacturer quoted the overall uncertainty in aethalometer data to be about 10%,

which is calculated by comparing the data of the aethalometer to other instruments that measure BC using different techniques [2]. However, Weingartner et al. [89] reported that BC measurements using filter techniques have significant uncertainty due to "shadowing effect" after investigating several types of carbon aerosols. This effect causes underestimation of BC measurement due to its high loading on the filter. This effect is very pronounced for pure BC while almost negligible for aged atmospheric aerosols. This uncertainty is found to be less than 10% [14].

2.2. Space-borne measurements

2.2.1. MODIS

AOD over Mt. Abu is also obtained from observations of the Moderate Resolution Imaging Spectroradiometer (MODIS) sensors on-board Terra and Aqua satellites. Terra and Aqua spacecrafts pass over the equator at 10:30 and 13:30 Local Solar Time, respectively [43]. Global images of the full disc are produced due to larger swath widths and instrument-scanning angle of $110°$ [44]. MODIS has 36 channels spanning the spectral range from 0.41 to 14.4 μm at three spatial resolutions: 250 m (2 channels), 500 m (5 channels) and 1 km (29 channels). MODIS aerosol algorithm consists of three independent algorithms to retrieve the aerosol characteristics, two over land and one over oceans, and makes use of eight of these channels (0.47-2.13 μm) [29, 35, 67]. The measurements at other wavelengths provide information to identify clouds and river sediments [20, 45]. MODIS provides an accurate retrieval of spectral AOD and the parameters characterizing aerosol size [79, 80]. The retrieved data used in this study include both Terra and Aqua MODIS aerosol products; such estimations are made over cloud-free regions only [67]. Long-term analysis of MODIS aerosol retrievals collocated with AERONET measurements confirm that MODIS retrieved AOD agrees with AERONET observations to within 0.10 over land and to within 0.035 over oceanic island sites. There are several studies demonstrating that MODIS AOD has a strong correlation with AERONET AOD [41, 83, etc.] and thereby provide enough confidence to use the MODIS AOD over western India, the region of interest in the current study.

2.2.2. OMI

Aerosol index (AI) is obtained from observations in the UV region (UV-1, 0.270 to 0.314 μm; UV-2, 0.306 to 0.380 μm) of the Ozone Monitoring Instrument (OMI) on-board Aura satellite [82]. AI is defined as the difference between satellite measured (including aerosol effects) spectral contrast at 0.360 and 0.331 μm radiances and the contrast theoretically calculated from radiative transfer model for pure molecular (Rayleigh) atmosphere [9, 25, 28]. The Aura satellite launched in July 2004, flies eight minutes after the Aqua satellite as a part of NASA A-train constellation. OMI has been designed for the replacement of Total Ozone Mapping Spectrometer (TOMS) to continue recording the total ozone and other atmospheric parameters related to ozone and climate study. OMI is sensitive to aerosol absorption even when aerosols are present above the cloud. Therefore, AI can be successfully derived for clear as well as cloudy conditions. OMI has a spatial resolution of 13×24 km at nadir and uses the same algorithm that is used for TOMS observations. AI provides a quantitative measurement of UV-absorbing aerosols over all the terrestrial surfaces including deserts and ice sheets. AI is positive for absorbing aerosols and negative for non-absorbing aerosols. Zero AI indicates cloud presence. High OMI-AI values with high MODIS-AOD and low Ångström exponent

represent dust dominated regions and such high AI values are mainly observed over arid regions [78]. OMI-AI Level 3 global-gridded product with spatial resolution of $0.25° \times 0.25°$ is obtained over western India for identifying the dust dominating periods in the present study.

2.2.3. CALIOP

The Cloud-Aerosol Lidar and Infrared Pathfinder Satellite Observations (CALIPSO) provides a new insight into the role of atmospheric aerosols and clouds in regulating the study of Earth's climate change and air quality. It is a part of the A-train satellite constellation that includes Aqua, CloudSat, and Aura satellites. CALIPSO is in a sun-synchronous orbit at 705 km at an inclination of $98°$ and provides the vertical distribution of aerosols and clouds. It consists of three sensors: a Cloud-Aerosol Lidar with Orthogonal Polarisation (CALIOP), an Imaging Infrared Radiometer (IIR), and a moderate spatial resolution Wide Field-of-view Camera (WFC). CALIPSO passes over the equator at 13:31 local hours, one minute behind Aqua. The primary instrument, CALIOP, transmits linearly polarized laser light of 0.532 μm and 1.064 μm at a pulse rate of 20.16 Hz. Its receiver measures the backscattered intensity at 0.532 μm and 1.064 μm with the former divided into two orthogonally polarized components which help to calibrate the optically thick clouds and aerosols. CALIOP observes both clouds and aerosols at high spatial resolution, but must be spatially averaged to increase signal to noise ratio. From the surface to 8 km, the vertical resolution is 30 m and the nominal horizontal resolution is 1/3 km. CALIPSO data products provide the aerosol vertical distribution along with aerosol layer height and AOD [7, 85]. CALIPSO LEVEL 2 Vertical Feature Mask (VFM) products provide vertical mapping of the locations of aerosols and clouds together with information about the types of each layer and the discrimination between aerosols and clouds is expected to be good in these products [4, 52, 87, etc.].

2.3. Models

2.3.1. OPAC

OPAC (Optical Properties of Aerosols and Clouds) model [26] is used to derive aerosol optical depth from the measured atmospheric aerosol chemical compositions obtained from literature [39, 40] at Mt. Abu. OPAC model contains two major parts: (1) a dataset of microphysical properties and the resulting optical properties of cloud and aerosol components at different wavelengths and for different humidity conditions, (2) a FORTRAN program that allows the user to extract data from this dataset, to calculate additional optical properties, and to calculate optical properties of mixtures of the stored clouds and aerosol components. In the present study, OPAC model has been used for obtaining the aerosol optical properties in shortwave region (0.25-4 μm) from the known chemical compositions. OPAC, based on Mie theory, can compute aerosol optical properties at 61 wavelengths starting from 0.25 μm to 40 μm. It mainly has 10 aerosol components which are as follows - insolubles (mostly soil particles), water soluble aerosols (mainly sulfate and nitrate aerosols of anthropogenic origin), soot (of anthropogenic origin), sea salts (naturally produced on the oceanic surface by wind and also available in the atmosphere of coastal regions) in accumulation and coarse mode, mineral dust (generally coming into atmosphere from the arid surface by wind) in three modes, transported mineral dust and sulfate droplets (mainly found at stratospheric altitudes). This model is used to derive the AOD spectrum using a combination of aerosol components and in the present study the sulfate droplets are not considered. Some of the aerosol components which

are hygroscopic in nature, may change their optical properties, and hence OPAC outputs are available for eight different relative humidity (0%, 50%, 70%, 80%, 90%, 95%, 98% and 99%) conditions. Optical properties for different aerosols are different. Single scattering albedo (SSA) is one of the important optical parameters for aerosol radiative effect calculations. OPAC derived SSA is the weighted average of SSA of all aerosol components. Water soluble (SSA $\approx$ 0.9 at 0.5 μm) aerosols which contain mainly sulfate, nitrate, etc. and seasalt (SSA $\approx$ 0.99 at 0.5 μm) do not absorb significantly in the visible range but they do absorb significantly in the infrared region (SSA $\leq$ 0.4 at 10.0 μm). Major aerosol components are scattering type in the shortwave range (0.25-4.0 μm), whereas, in the longwave range (4.0-40.0 μm) they can be totally absorbing. The SSA of soot in the shortwave is 0.22 (at 0.5 μm), whereas, in the longwave range it is totally absorbing. Dust (SSA $\approx$ 0.98 at 0.5 μm) is mainly scattering in nature in the shortwave range but exhibits strong absorption in UV region and also in the longwave range. On one hand, in the longwave region absorption decreases the outgoing radiation, while on the other hand, the energy re-emitted consequent to this absorption increases the surface reaching infrared radiation. The net SSA over a particular location is the weighted average of SSA of all aerosol components.

2.3.2. SBDART

Atmospheric radiative transfer code, named Santa Barbara DISORT Atmospheric Radiative Transfer (SBDART) [68] developed at the University of California, Santa Barbara, is used to estimate aerosol radiative forcing over the study area. SBDART is a well established code for estimation of radiation flux in the shortwave (0.25-4.0 μm) as well as longwave (4.0-40.0 μm) range. It is a radiative transfer code that computes plane-parallel radiative transfer in clear and cloudy conditions within the Earth's atmosphere and at the surface. In the present study only clear sky conditions are considered. All the important processes that affect the ultraviolet, visible, and infrared radiation, are included in this code. For molecular absorption SBDART uses the low-resolution band models of LOWTRAN-7 atmospheric transmission code [56]. LOWTRAN-7 codes can take into account the effects of all radiatively active molecular species found in the Earth's atmosphere with wavelength resolution of about 5 nm in the visible and about 200 nm in the thermal infrared. In SBDART, the radiative transfer equations are numerically integrated with DISORT (Discreet Ordinate Radiative Transfer) code [74]. This discrete ordinate method provides a numerically stable algorithm to solve the equations of plane-parallel radiative transfer in a vertically inhomogeneous atmosphere. The intensity of both scattered and thermally emitted radiation can be computed at different heights and directions. Presently, SBDART is configured to allow up to 65 atmospheric layers and 20 radiation streams (20 zenith angles and 20 azimuthal modes).

The ground surface cover is an important determinant of the overall radiation environment because spectral albedo of the surface which defines the ratio of upwelling to downwelling spectral irradiance at the surface determines upwelling irradiance from the surface. In SBDART there are five basic surface types, namely (1) ocean water [76], (2) lake water [36], (3) vegetation [65], (4) snow [91], and (5) sand [73]. The spectral albedo describing a given surface is often well approximated by combinations of these basic surface types. Input parameters in SBDART allow the user to specify a mixed surface consisting of weighted combinations of water, snow, vegetation and sand. SBDART can compute the radiative effects of several lower and upper atmosphere aerosol types. In the lower atmosphere, typical rural, urban,

or maritime conditions can be simulated using the standard aerosol models of Shettle & Fenn [72]. SBDART gives the opportunity to specify up to five aerosol layers (i.e., at five different altitudes), with radiative characteristics that model fresh or aged volcanic, meteoric, and upper-tropospheric background aerosols.

The major inputs required to estimate the aerosol radiative effects for DISORT module in SBDART include spectral values of solar radiation incident on the atmosphere, spectral values of columnar AOD, SSA and angular phase function of the scattered radiation or asymmetry factor. The asymmetry factor is used to generate a scattering phase function through the Henyey-Greenstein approximation. The Henyey-Greenstein parameterization provides good accuracy when applied to radiative flux calculations [22, 84]. It can also compute radiation fluxes with less uncertainty from the aerosol optical properties at 0.55 micron wavelength obtained from satellite observations. Spectral values of AOD, SSA and asymmetry parameter are also obtained from OPAC using the chemical properties of the atmospheric aerosols. OPAC model derived aerosol optical parameters are obtained by varying the number concentration of individual components in small steps until the model derived parameters satisfactorily match the observed values. Another important input parameter that is required for accurate computation of the aerosol radiative effects over land is the surface reflectance [71, 90]. Radiative forcing is determined from the difference of the solar radiation with and without aerosols during clear-sky conditions in the short wave (0.25-4.0 μm) by running SBDART for every one hour interval in a day using the profiles for tropical atmosphere. The present work gives more realistic results considering the aerosol vertical profiles from CALIPSO and MODIS surface reflectance over Mt. Abu. The seasonal forcing is estimated from the diurnally averaged forcing which represents the mean of the hourly forcing as derived from SBDART for 24 h/day.

3. Site location and meteorology

Major aerosol parameters have been monitored during 2006 and 2007 inside the campus of Physical Research Laboratory situated at Gurushikhar, Mt. Abu – the highest peak (1.7 Km asl) of Aravalli range in India. Topography of the Indian Peninsula, Himalayas and the Tibetan plateau are shown in Figure 1a. Arid (dashed line) and semi-arid (solid line) regions of Thar Desert in western India are shown in Figure 1b. More details on physical features of Thar Desert are described in literature [92]. Mt. Abu is situated within the semi-arid region of Thar Desert. A picture of the campus is shown in Figure 1c, which is better known for the astronomy observatory. Aravalli mountains are located in between Thar Desert and IGP. Major part of these mountains on the western side is in the semi-arid region of Thar Desert while the north-east region of the mountains is in IGP. The highest location, Mt. Abu is situated in the south-west of the mountain range. The observatory being a prohibited hilltop area makes the measurement site anthropogenic free and hence, is a suitable place for background aerosol measurements in western India. The observatory is built on rocky mountainous terrain surrounded by forest and therefore, there is significantly less soil dust coming from the surface of the nearby mountain region. Being very close (~300 Km) to Thar Desert, measurement site gives an opportunity to study desert dust. Freshly generated desert dust aerosols are transported within few hours to Mt. Abu and thereby are exposed to local pollutants minimally. Also, due to the high altitude, these aerosols are less influenced by the boundary layer aerosols that consist mostly of locally produced anthropogenic aerosols.
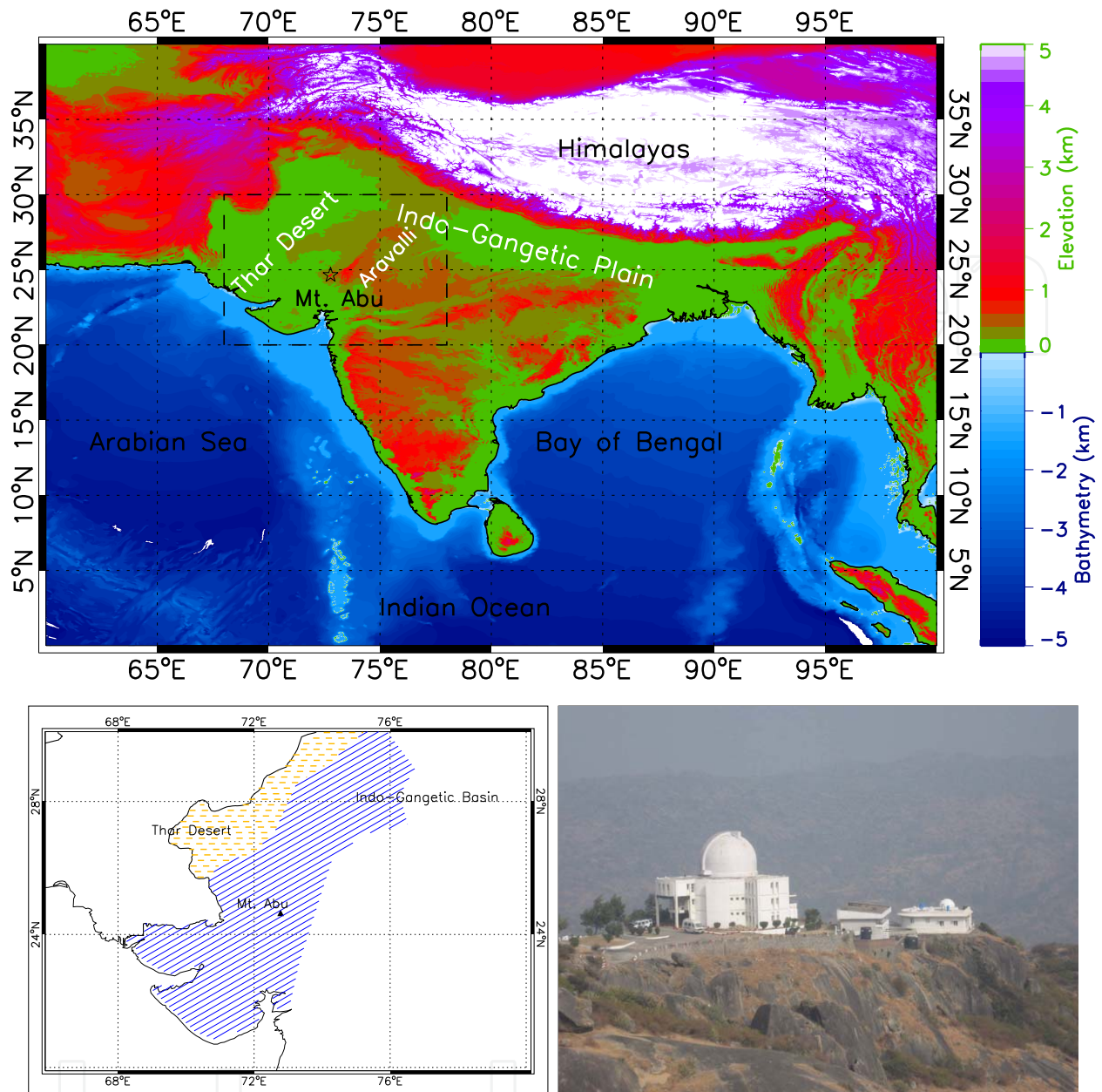
Figure 1. (a) Topography of the Indian subcontinent. The box is showing western India including Thar Desert and Indo-Gangetic Plain. Star shows the location of Mt. Abu, highest location in the Aravalli Mountains. (b) Arid (dashed lines) and semi-arid (solid lines) region of Thar Desert. Mt. Abu is situated in the semi-arid region. (c) A photograph of the measurement site - PRL observatory at Mt. Abu.

Diurnal variations of surface temperature and relative humidity (RH) at Mt. Abu during different seasons are shown in the top row of Figure 2. The vertical bars represent the $\pm 1\sigma$ variation about the hourly mean values. Temperature is found to be minimum at $15.5\pm3.0^\circ$C during winter and maximum at $23.0\pm3.3^\circ$C during premonsoon, followed by monsoon ($19.3\pm2.0^\circ$C) and postmonsoon ($18.3\pm1.4^\circ$C). In case of RH, minimum is observed at $24.6\pm6.4\%$ during premonsoon and maximum at $88.3\pm10.5\%$ during monsoon, followed by $54.7\pm22.8\%$ during postmonsoon and $30.7\pm8.3\%$ during winter. There is a strong diurnal variation in the hourly averaged surface temperature at Mt. Abu during all seasons, whereas,

there is no significant variation present in RH. During monsoon and postmonsoon RH shows large variations about the means. During monsoon all the measurements of aerosol parameters were carried out only in June (mean RH = 63.9±12.6%). Observations were very few in July and August due to heavy rain and high RH. The seasonal variation of wind pattern over India subcontinent, obtained from National Center for Environmental Prediction (NCEP) reanalysis data is shown in the bottom row of Figure 2. Wind speed over study region was minimum and mainly coming from IGP during winter,. During premonsoon, wind over western India was westerly and coming from desert areas. During monsoon and postmonsoon, wind became stronger coming from coastal region of Arabian Sea.
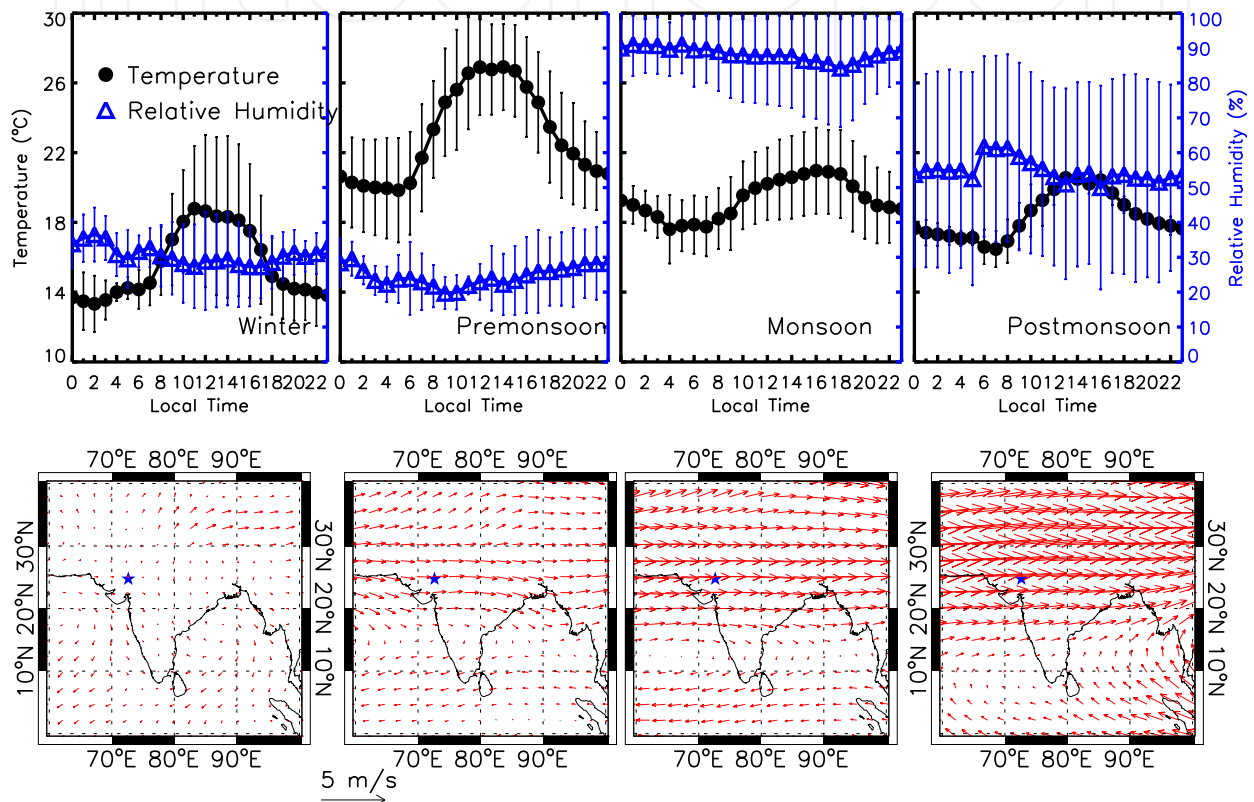

Figure 2. (Top) Diurnal variation of temperature and relative humidity during different seasons. The vertical bars represents ±1σ variation about the mean. (Bottom) Seasonal variation of wind speed and direction, obtained from NCEP reanalysis data.

3.1. Land surface properties

Underlying surface plays an important role in the aerosol radiative effects towards climate change [24, 27, etc.]. Aerosols over high surface reflectance (bright surface) can produce relatively higher positive radiative forcing than those over low surface reflectance (dark surface). Space-borne observations suggest that there is a strong seasonal variation of surface over western India. Figures 3a and 3b show images of land surface over western India during premonsoon and postmonsoon seasons, respectively, captured by MODIS-Terra satellite. The surface is very bright during premonsoon due to open bare land, while it is relatively dark

during postmonsoon due to green vegetation born during monsoon rain. As a result, surface reflectance is maximum during premonsoon and minimum during postmonsoon.

In the present study, MODIS derived surface reflectance data over Mt. Abu is used in the estimations of radiative forcing. It is obtained from Nadir BRDF-Adjusted Reflectance 16-Day L3 Global 0.5 km SIN Grid product which is derived at the mean solar zenith angle of Terra overpasses for every successive 16-day period, calculating surface reflectance as if every pixel in the grid was viewed from nadir direction. Surface reflectance data available in seven wavelength bands of MODIS centered around 0.47, 0.56, 0.65, 0.86, 1.24, 1.64 and 2.13 μm are used to reproduce the spectral dependence of surface reflectances for the entire SW range using a combination of three different surface types, namely, vegetation, sand and water. The monthly variation of surface reflectance at 1.64 μm during 2007 is shown in Figure 3c. Vertical lines in this Figure represent $\pm 1\sigma$ variation about the monthly mean values. Average surface reflectance is found to be high at about 0.35 during premonsoon (Apr-May) and low at about 0.20 during postmonsoon (Sep-Nov) and winter (Dec-Feb). Space-borne observations show that the land over western India increases its brightness by about 75% during premonsoon season. This could be due to bare surface and deposited dust that is transported from arid region. Model simulations to fit the surface reflectance combining the three surfaces suggest that during premonsoon sand surface contributes a maximum of about 70% and during postmonsoon and winter it contributes a minimum of about 20% while vegetation surface contributes 15% and 60%, respectively. These varying land properties are also considered in the radiative forcing calculations.

4. Background aerosol optical and physical properties over Thar desert

4.1. Aerosol optical depth

The seasonal variation of AOD spectrum at the hilltop station over western India is shown in Figure 4. Vertical lines represent $\pm 1\sigma$ variation about the mean AOD. The solid lines are the OPAC model fitted AOD spectrum and the shaded regions indicate the variation of simulated AOD within that season. At all wavelengths, AODs are maximum during premonsoon followed by postmonsoon and monsoon and are minimum during winter. At 0.5 μm, the AODs are 0.20$\pm$0.08, 0.18$\pm$0.04, 0.10$\pm$0.02, and 0.08$\pm$0.03 during premonsoon, postmonsoon, monsoon and winter, respectively. The reasons could be as follows. Firstly, there is a large variation of boundary layer height. In an earlier research work carried out over a tropical Indian station, Gadanki (13.5^{o}N, 79.2^{o}E), Krishnan & Kunhikrishnan [37] studied the annual boundary layer height variation and observed a minimum during winter and maximum during premonsoon. In the present study, during winter the boundary layer height is lower than the observation altitude and hence the observation site is in the free troposphere region. As a result, AOD is minimum during this season. During premonsoon the observation site is within the boundary layer and hence AOD increases. In addition, there is significant amount of dust transported from arid region which results in maximum AOD. On the other hand, during monsoon though the boundary layer height is significantly high, AOD is low due to wash out of aerosols from the atmosphere by the heavy monsoonal rain events. Monsoon rain has a major role to wash out the aerosol loading from the atmosphere causing significant decrease of AOD. A case study over tropical Indian station reported about 64% decrease of AOD due to heavy rain [69]. In the present study, there is no significant decrease of AOD during monsoon. This is because of the presence of a very stable aerosol layer of about 1.5
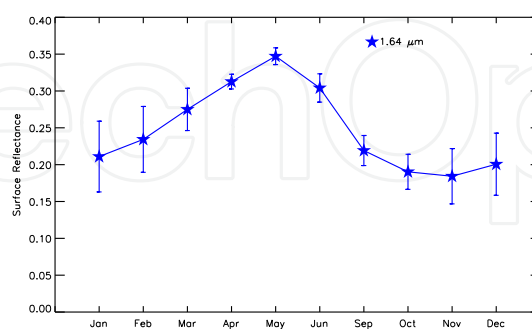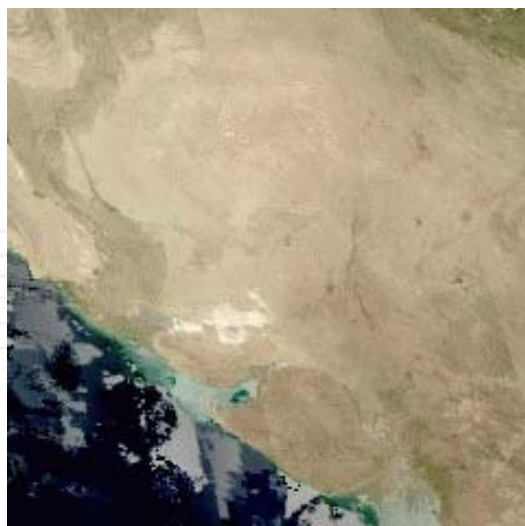
Figure 3. Picture of land surface over western India during premonsoon (top) and potmonsoon (middle) seasons, obtained from MODIS-Terra satellite. Dark black, gray and green colors represent oceanic surface, arid bare land, forest regions, respectively. (Bottom) Monthly variation of surface reflectance at 1.64 μm wavelength during 2007 and the vertical bars represents $\pm 1\sigma$ deviation about the monthly mean. Note that the surface reflectance increases by 70% over study area during premonsoon.

km thickness over the inversion layer during monsoon in the western India, as reported by Ganguly et al. [19].

The spectral dependence of AOD is parameterized through Ångström exponent (α) which is the slope of the logarithm of AOD versus the logarithm of wavelength (in micron) and provides the basic information about the columnar particle size distribution [66]. α is higher for relatively higher number of smaller particles and as the number of bigger particles increases α decreases. It can even reduce to ∼0 for very large number of coarse-mode soil particles [51, 77, 81, etc]. In the present study, α is obtained from Microtops measured AOD for the entire wavelength (0.380 - 1.020 μm) and is given in Figure 4 along with the variation in the parenthesis. It varies from 0.2 to 0.6. During monsoon α is minimum at 0.2±0.15 indicating dominance of bigger aerosols. It is due to the presence of bigger water soluble aerosols which increase in size due to accumulation and coagulation processes in high relative humidity conditions. During premonsoon also, when RH is low and the atmosphere is dry and warm, α is low at about 0.3±0.25 indicating the dominance of bigger aerosols. These are the soil born dust aerosols produced by the frequently occurring dust storms in the Thar desert and transported to other parts of India [17, 55] including Mt. Abu. α is found to be maximum at about 0.6±0.01 during postmonsoon indicating dominance of smaller aerosols. This is probably due to dominance of fine seasalt aerosols transported from Arabian Sea [19, 64] . During winter also α is found to be high showing dominance of smaller aerosols which could be due to anthropogenic aerosols coming from burning tree branches and dry leaves by the poor villagers living in the surrounding hill areas to keep themselves warm during cold mornings and evenings.

4.2. Aerosol mass concentration

Aerosol mass concentration measured separately in ten different sizes by Quartz Crystal Microbalance (QCM) cascade impactor has been classified into three different categories, viz., nucleation (radius<0.1 μm), accumulation (0.1μm≤radius≥1.0 μm) and coarse (radius>1.0 μm) mode particles. Nucleation mode aerosols represent total aerosols collected in stages 9-10, accumulation mode aerosols are the total aerosols in stages 5-8 and coarse mode aerosols are the total aerosols collected in stages 2-4. Aerosols collected in stage 1 are not considered in the calculations because all aerosols whose radius is greater than 12.5 μm are collected in this stage and thus, there is no definite aerosol radius representing this stage.

Figure 5 shows the seasonal variation of aerosol mass concentration (μg.m^{-3}) of all three modes, viz., nucleation, accumulation and coarse modes at the hill top region, Mt. Abu from January 2006 to December 2007. Total aerosol mass concentration observed was minimum at 16.5±1.5 μg.m^{-3} during winter and maximum at 25.8±2.7 μg.m^{-3} during postmonsoon followed by premonsoon (19.9±5.6 μg.m^{-3}) and monsoon (16.7±6.0 μg.m^{-3}). This variation is similar to that observed in columnar AOD at Mt. Abu. The accumulation aerosol mass was contributing maximum to the total aerosol mass during all seasons and the coarse mode aerosol mass was contributing equivalently only during premonsoon. This is due to large transportation of dust aerosols from Thar desert during this season that enhanced the coarse mode aerosol mass.

In general, nucleation aerosols contribute least to the total aerosol mass concentration. This contribution was maximum during postmonsoon when the wind speed was almost calm and RH was relatively high. This atmospheric condition helps in gas-to-particle conversion and
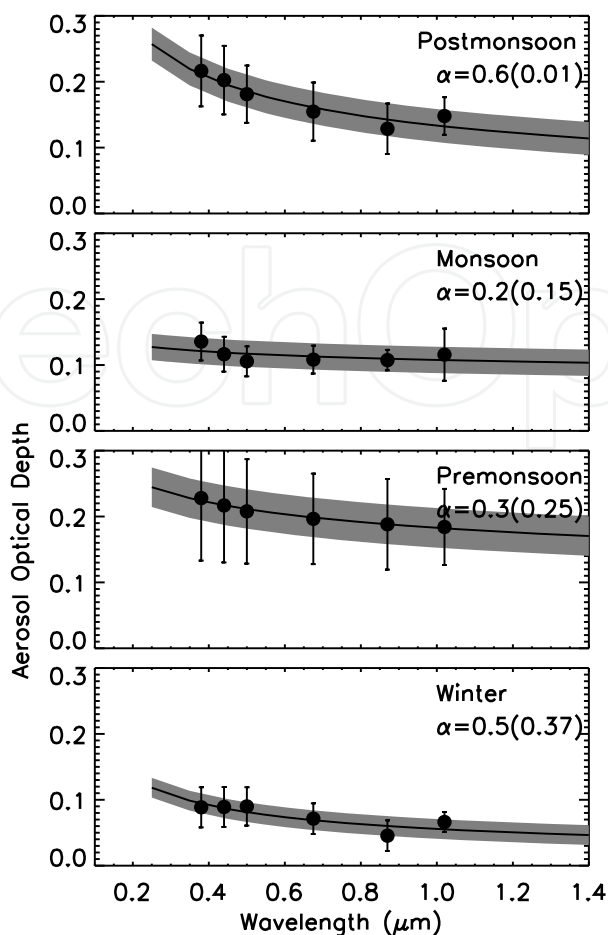
Figure 4. Seasonal variation of observed AOD spectrum at Mt. Abu. Vertical bars represent $\pm 1\sigma$ variation about the mean. Solid line is the OPAC model derived AOD spectrum and the shaded regions are the variation in the simulated AOD. Ångström exponent (α) is also given along with the standard deviations in parenthesis.

enhances the nucleation mode aerosols which explains the maximum mass of 6.4 ± 1.1 $\mu g.m^{-3}$ observed during this season. During winter the nucleation mass concentration decreased to 3.2 ± 0.1 $\mu g.m^{-3}$ as the boundary layer height decreased and the measurement site was in free troposphere. The nucleation aerosol mass was 2.9 ± 1.8 and 3.6 ± 0.7 $\mu g.m^{-3}$ during premonsoon and monsoon, respectively. During premonsoon, the boundary layer height was maximum which gives more room for these fine aerosols to dilute and high temperature with low RH are not favorable for gas-to-particle conversion processes. In addition, strong wind also helps in removing the aerosols from the measurement site during this season and makes mass of the nucleation mode aerosols minimum. Monsoon also experiences high boundary layer height and strong wind condition, however, nucleation mode aerosols are significant compared to premonsoon. This could be due to the transport of seasalt coming from Arabian Sea.

The seasonal variation observed in the accumulation aerosols is similar to the nucleation aerosols. The accumulation aerosol mass concentration was minimum at 8.4 ± 2.8 $\mu g.m^{-3}$ during premonsoon and maximum at 12.6 ± 0.6 $\mu g.m^{-3}$ during postmonsoon followed by monsoon (10.0 ± 1.0 $\mu g.m^{-3}$) and winter (9.6 ± 1.6 $\mu g.m^{-3}$). Accumulation aerosols are mainly produced by the condensation growth and coagulation of nucleation aerosols. During
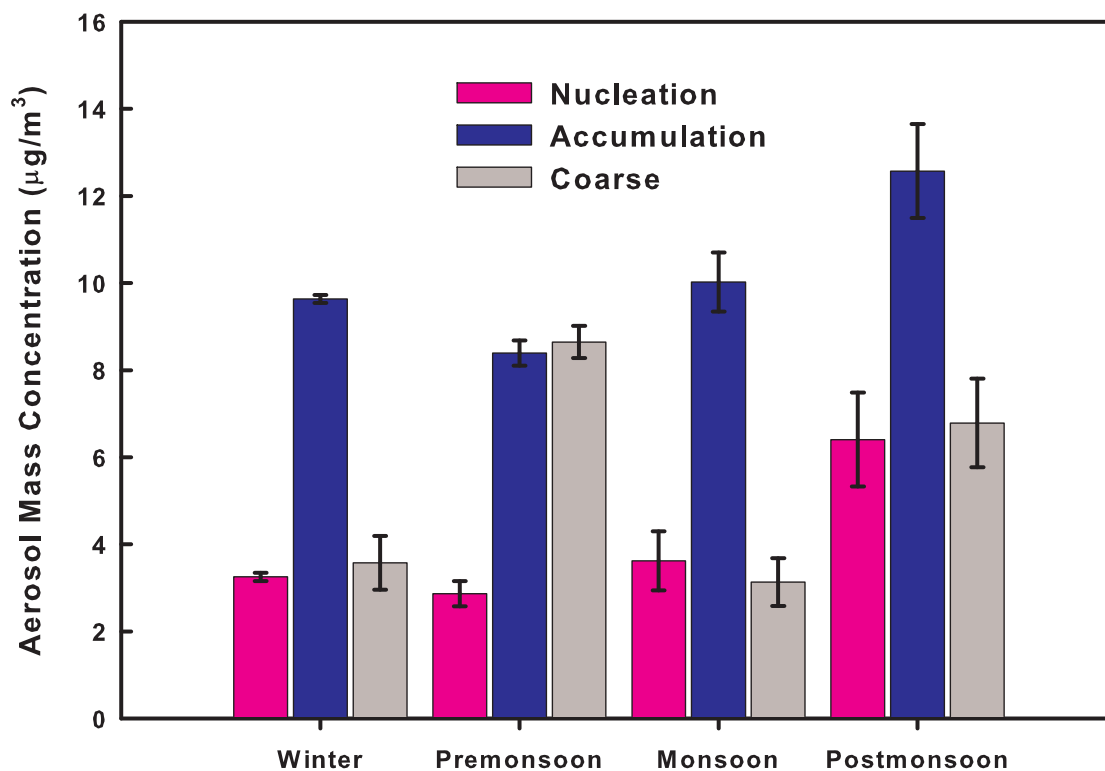
Figure 5. Seasonal variation of aerosol mass concentrations in nucleation (radius < 0.1 micron), accumulation (0.1≥radius≤1.0 micron) and coarse (radius >1.0 micron) modes. The vertical bars represent $\pm 1\sigma$ variation about the mean.

premonsoon these processes are slowed down due to low RH and hence the low accumulation aerosol mass. During monsoon seasalt aerosols are transported from the Arabian sea and high RH maintains the accumulation mode aerosols, increasing the mass concentration. During postmonsoon, minimum wind speed results in further increase resulting in the observed maximum. And during winter it is minimum as the the measurement site is in the free troposphere.

The coarse mode aerosols show a slightly different seasonal behaviour at Mt. Abu. During premonsoon, they mainly consist of dust aerosols transported from Thar desert and the mass concentration is maximum at 8.6±0.4 μg.m^{-3}. It is minimum at 3.1±0.5 μg.m^{-3} during monsoon due to wash out of the dust aerosols by heavy rains. During postmonsoon, the coarse aerosol mass concentration was slightly enhanced to 6.8±1.0 μg.m^{-3} as the accumulation aerosols, which mainly consist of seasalt particles, swell up by absorbing water vapor at high RH conditions and become coarse mode particles. During winter, their mass concentration becomes 3.6±0.6 μg.m^{-3} when low boundary layer height helps to keep them low at the hill-top region.

4.3. Aerosol number concentration

Aerosol number concentration is also obtained from the observed aerosol mass concentration from QCM observations for the hilltop area using appropriate mass density valid for semi-arid background atmosphere and prevailing relative humidity conditions [13, 26]. Figure 6 shows

the typical aerosol size distributions for the four seasons. The vertical bars represent $\pm 1\sigma$ variation about the monthly mean number concentration of different sizes of aerosols. In all seasons, the size distribution showed tri-modal distribution and each mode could be fitted using using three lognormal modes of the following form.

$$\frac{dn\,(r)}{dr} = \frac{N}{\sqrt{2\pi}\log\sigma_m}\exp\left[-\frac{\log^2\left(\frac{r}{r_m}\right)}{2\,(\log\sigma_m)^2}\right] \tag{2}$$

where N is the number concentration (cm^{-3}), σ_m is the width of the distribution and r_m is the mode radius for a particular mode. The three modal parameters for all the seasons are given in Table 1. At Mt. Abu the number concentrations (N) of nucleation and accumulation modes are lower by an order of magnitude than that at other urban region in western India, Ahmedabad while for coarse mode it is comparable [19]. Since Mt. Abu is far from anthropogenic activity, the anthropogenically influenced modes (nucleation and accumulation) have smaller number concentrations. However, the proximity to Thar desert and similarity of the surface conditions of Mt. Abu make the coarse mode number concentrations comparable. The radii of nucleation mode lie in the range 0.018-0.020 μm and number concentration for this mode is found to be maximum during postmonsoon and minimum during premonsoon and monsoon. Similarly the radii for corresponding accumulation and coarse modes lie in the range of 0.12-0.19 μm and 1.1-2.1 μm, respectively.

Season	Nucleation			Accumulation			Coarse		
	N	r_m	σ	N	r_m	σ	N	r_m	σ
	cm^{-3}	μm	μm	cm^{-3}	μm	μm	cm^{-3}	μm	μm
Winter	12000	0.019	2.0	18	0.14	2.0	0.02	1.4	1.9
Premonsoon	10000	0.018	1.9	22	0.19	1.8	0.01	2.2	1.8
Monsoon	15000	0.018	1.9	50	0.13	1.9	0.01	1.7	1.8
Postmonsoon	17000	0.020	1.9	60	0.12	1.9	0.08	1.1	1.8

Table 1. Average values of size distribution parameters obtained by fitting lognormal curves to the measured aerosol number distribution over Mt. Abu

Accumulation aerosols are mainly produced by the condensation growth and coagulation of nucleation aerosols. During winter accumulation mode aerosols number concentration (N) was minimum at 18 cm^{-3}. During premonsoon, the anthropogenic activities were maximum at Mt. Abu which increased N of accumulation mode to 22 cm^{-3}. During monsoon, it further increased to 50 cm^{-3}. It is due to the wind coming from Arabian sea (Figure 2) that carried large amount of sea salt and enriched the sea salt aerosols at the hill top region [64]. During high RH conditions these sea salt aerosols belong to the accumulation mode. Later during postmonsoon, wind was south-easterly and the transported sea salt reduced. However, burning of biomass like garbage and fallen leaves increased and hence, BC particle concentration was enhanced. Therefore, high production, shallow boundary layer height and low wind speed made the accumulation mode aerosol number concentration reach a maximum at 60 cm^{-3} during this season.

During premonsoon, there is large transportation of mineral dust aerosols from Thar Desert which enhanced the abundance of coarse mode aerosols at the hill top area. The coarse mode radius was maximum at 2.2 μm. During monsoon, rain washes out these dust aerosols from the atmosphere and reduces their number and mode radius. However, the abundance
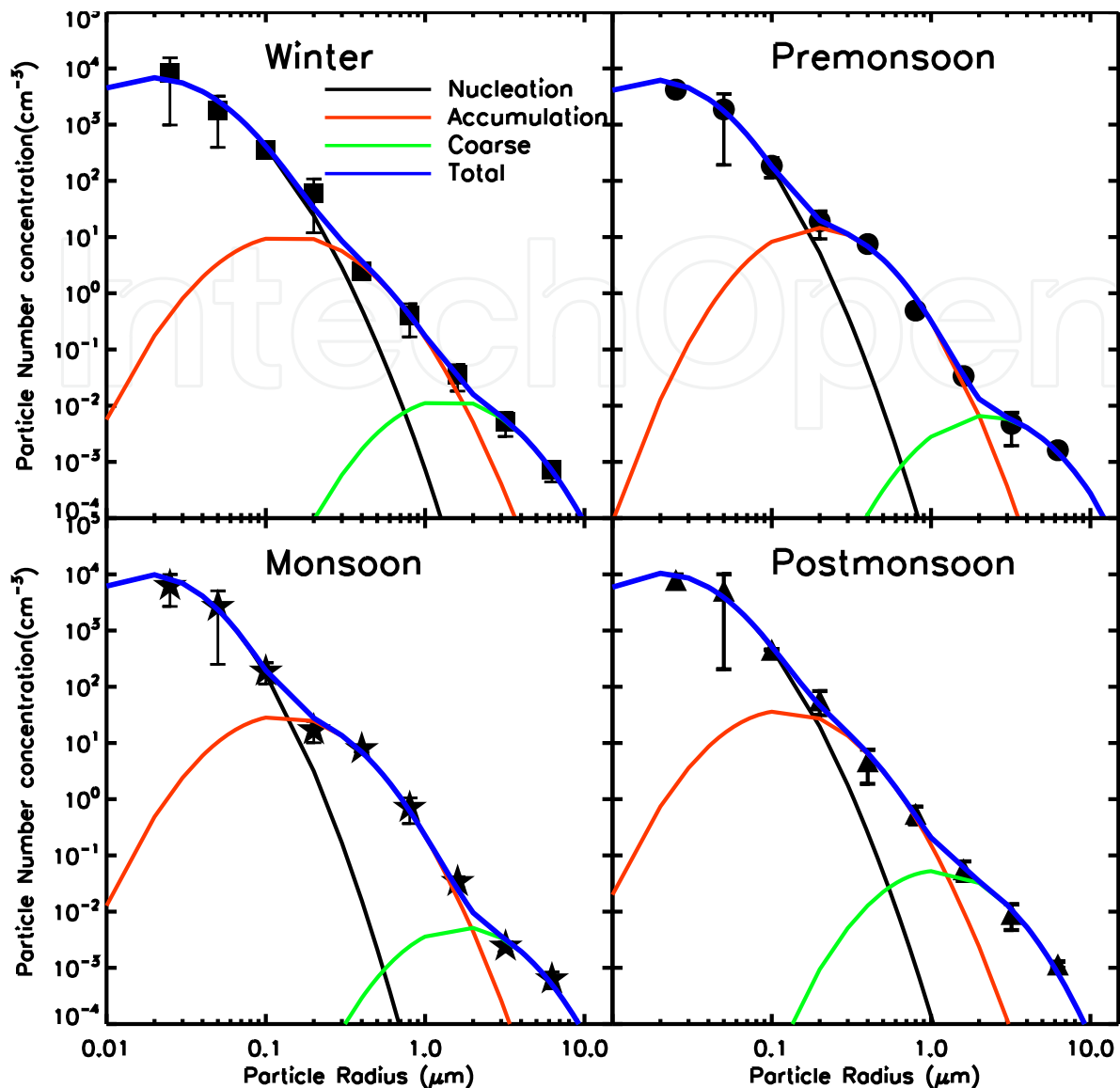
Figure 6. Seasonal variation of aerosol number distribution. Vertical bars represent $\pm 1\sigma$ variation about the mean. The solid lines are the best-fitted curves representing nucleation, accumulation and coarse modes.

of coarse aerosols is found to be maximum with minimum mode radius of about 1.1 μm during postmonsoon which indicates the transfer of aerosols from accumulation mode due to hygroscopic and coagulation growth of particles at high RH conditions.

4.4. Black carbon mass concentration

Black carbon (BC) produced due to incomplete combustion of carbon-based fuels [3, 31, 53, 86, etc] is the most efficient light absorbing aerosol component in the atmosphere. BC has major contribution to alter the radiative balance by absorbing the solar radiation in the visible spectrum. As a result, it cools the surface and warms the atmosphere [24, 38]. A recent study of BC contribution to radiative forcing by Jacobson [31] showed that BC has a great contribution towards global warming and is the second most important component of global warming

after CO_2 and has a larger impact on direct radiative forcing than that of methane. As a result, in populated countries like China and India, the large production of BC aerosols has a large impact on the hydrological cycle and precipitation pattern [46, 61, 71]. In India the fraction of BC production from fossil fuel burning, open burning and biofuel combustion to the global emission is significantly large and hence, it is necessary to estimate radiative impact of different kinds of BC not only on global scale but also in the regional scale.
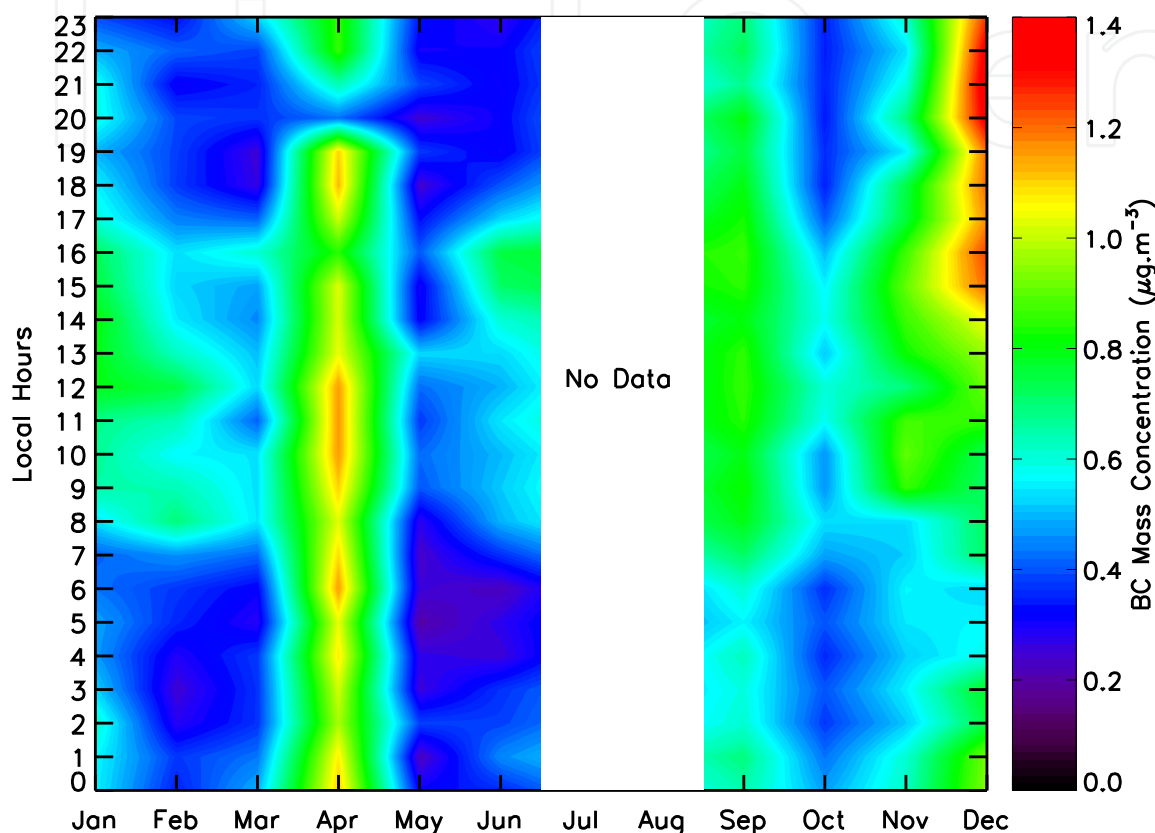

Figure 7. Diurnal variation of BC mass concentration during each month in 2007. White region indicates no data during Jul-Aug due to heavy monsoonal rain.

In recent years, global climate has received considerable attention due to increase in the percentage contribution of anthropogenic aerosols on the Earth's radiation budget [23]. BC particles exist mainly in the accumulation mode and can be transported over long distances [12] from source regions to far off pristine environment and perturb the climate of the latter, like that of Mt. Abu. The diurnal variation of BC mass concentration during different months over Mt. Abu is shown in Figure 7. Observations were not possible in July and August due to heavy rain. Minimum BC concentration was observed during monsoon (0.428 ± 0.128 $\mu g.m^{-3}$) and maximum was observed during premonsoon (0.665 ± 0.478 $\mu g.m^{-3}$) followed by winter (0.608 ± 0.246 $\mu g.m^{-3}$) and postmonsoon (0.620 ± 0.158 $\mu g.m^{-3}$). The annual mean BC mass concentration was 0.580 ± 0.104 $\mu g.m^{-3}$. At Mt. Abu the BC concentration is an order of magnitude less than that at any other urban region in India. BC during April is found to be as high as 1.00 ± 0.170 $\mu g.m^{-3}$ which is a factor of 2 higher than the previous month. Backtrajectory analysis indicates wind coming from IGP which increases the BC concentration. In another study at a high altitude station, Nainital (29.4^oN, 79.5^oE, 1950m

asl), in central Himalayas, mean BC was observed to be 1.36$\pm$0.99 μg.m^{-3} during December 2004 [55]. This shows that Mt. Abu is less affected by anthropogenic activities.

The diurnal variation of BC mass concentration does not show any significant morning and nocturnal peaks like other urban regions. However, increased BC was observed during the noon hours except during November and December. The reason for such an increase is during the day time the thermal convection becomes stronger and as a result, the pollutants at the foothill area rise up to the hilltop region and enhance the BC concentration. This day time enhancement was prominent during winter and postmonsoon because during these seasons there is a large difference between the day and night time temperatures. During November and December the night time BC concentration was larger by a factor of two. During these months the nearby villagers burn wood and fallen leaves to keep themselves warm thereby increasing the BC mass concentration. During January this nocturnal enhancement was not observed. The reason is that the boundary layer height is less than the station altitude and the night time BC that is produced cannot reach the hill top region due to weak thermal convection. During this period hill top region becomes pollutant free region.

5. Satellite observed aerosol properties over Mt. Abu region

5.1. Aerosol optical and physical properties

In the current satellite era, large databases are available to study aerosol properties from space, both in the regional and the global scale, that are essentially demanding. For the present study, Terra and a series of satellite sensors flying on the A-train platform provide the required data. MODIS on board Terra and Aqua provide aerosol parameters in the morning and afternoon. OMI on board Aura satellite provides AI. The joint information of AOD, Ångström exponent (α) and small mode fraction (SMF) retrieved from MODIS and AI retrieved from OMI can be utilized to estimate the optical properties of aerosols with their size and type. In addition, the aerosol vertical distribution obtained from CALIPSO fulfills the requirement for the regional climate change study. In the present study, AOD, α, SMF and AI obtained from above multi-satellite observations are considered to distinguish the dominant natural and anthropogenic aerosols during different seasons. Figure 8 shows the multi-satellite observed AOD, α, SMF and AI over the study area during 2006–2007. Open circles represent the parameters obtained from MODIS-Aqua and filled circles are MODIS-Terra observations. AI gives information about the dust aerosols while SMF provides information about the anthropogenic and natural aerosols. Low SMF with low α indicates the presence of natural aerosols and the reverse represents the dominance of anthropogenic aerosols. AI has large values during Mar-Jul, whereas, α and SMF have low values. These combined observations suggest the abundance of coarse dust aerosols during these periods. OMI captures many dust storms over Thar Desert during premonsoon season in the AI images and enhancement of AI is due to transport of the dust plume from the desert region. During Aug-Feb, SMF is found to be high and AI is found to be very low indicating less abundance of dust aerosols in the atmosphere. In addition, α is also found to be very low during Aug-Sep but AOD is significantly high. Earlier studies from chemical composition of aerosol samples collected at Mt. Abu reported the enhancement of seasalt aerosols transported from Arabian sea during these periods and ground-based lidar observations at Ahmedabad, located 300 km to the south of Mt. Abu, reported the existence of a layer of seasalt aerosol in between 2–4 km [19, 64]. It can thus be inferred that the increase of monsoonal AOD is due to transport

of seasalt aerosols from Arabian Sea. During Oct-Feb, high values of α are found indicating enhancement of anthropogenic aerosols. Ground-based observations show high abundance of BC on the hill-top region during winter. All these observations suggest that dust is dominating during premonsoon, anthropogenic aerosols during winter and natural seasalt are present in the atmosphere during monsoon season.
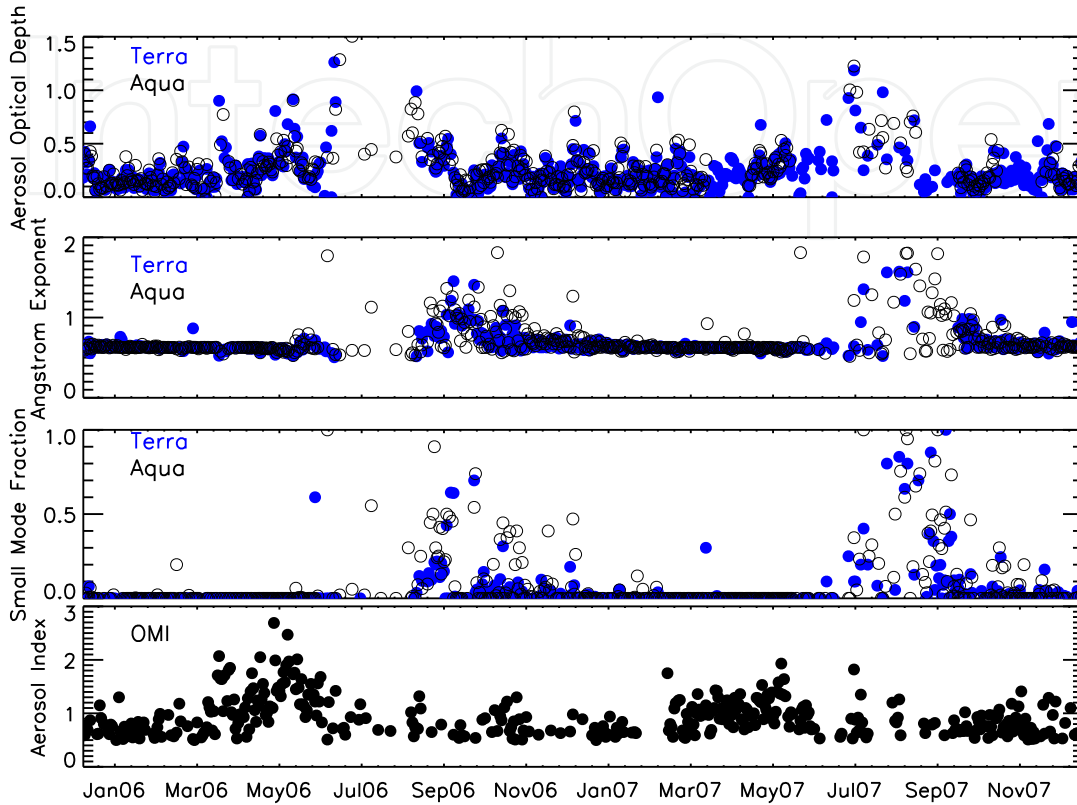

Figure 8. Space-borne daily observations of AOD, Ångström exponent, small mode fraction (SMF) obtained from MODIS onboard Terra and Aqua satellites and aerosol index obtained from OMI onboard Aura satellite during 2006 and 2007.

5.2. Aerosol vertical profile

Seasonal variation of aerosol vertical profiles over the study region is obtained from CALIPSO observations. Figure 9 shows the seasonal variation of aerosol extinction coefficient (km^{-1}). The horizontal dotted line at 1.7 km represents the height of Mt. Abu. The extinction coefficient is directly proportional to the total aerosol loading. It is clearly seen from the figure that aerosol loading over Mt. Abu is minimum during winter and higher during other seasons. There is a peak found near 2.2 km altitude during monsoon which becomes weak during postmonsoon. Ganguly et al. [19] reported that this peak is due to seasalt aerosols transported from Arabian sea and chemical analysis also supports this result showing significantly high amount of seasalt present over Mt. Abu during monsoon [64]. During premonsoon, there is a peak at 4.2 km which is due to the transported dust layer. MODIS and OMI observations also indicate significant amount of dust present in the atmosphere.

Near surface region also shows high extinction coefficient values. This could be due to locally produced anthropogenic aerosols. In the present study, the properties of aerosols at the
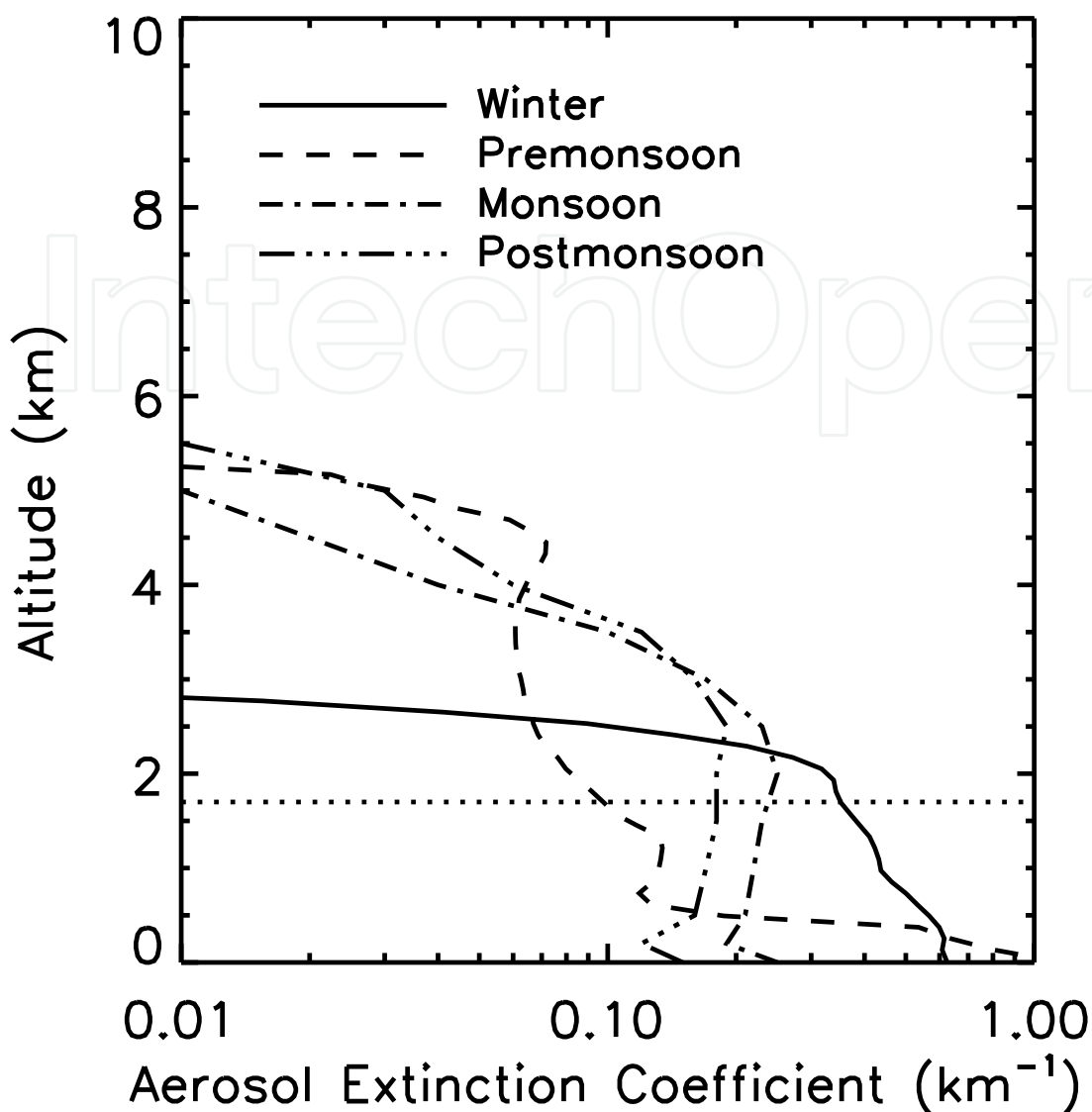
Figure 9. Seasonal variation of vertical distribution of aerosol extinction coefficient obtained from CALIPSO observations. The horizontal dashed line at 1.7 km is the altitude of Mt. Abu.

hill-top region are considered and defined as the 'background aerosols'. The vertical profile of aerosols indicate that these background aerosols are less influenced from these locally produced anthropogenic aerosols. Therefore, the aerosol properties observed over Mt. Abu are assumed to represent those of the background aerosols over semi-arid region of western India.

6. Natural and anthropogenic background aerosol properties

6.1. Estimation of natural and anthropogenic aerosols

The estimation of natural and anthropogenic aerosols over this background site is a challenging task because many aerosol compositions have both origins. For example, sulphates are mainly considered as anthropogenic components over urban regions as they

are coming from factories and vehicular emissions. However, there is significant contribution from marine sources as di-methyl sulphate. On the other hand, BC is mainly anthropogenic, but it becomes natural when produced during natural forest fires. In the present study, dust and seasalt are considered as natural aerosols and BC, sulphate and nitrates as anthropogenic aerosols. BC is obtained from ground-based measurements using Aethalometer. Other aerosols like dust, sulphate and nitrates are obtained from the chemical analysis of aerosols samples collected over this hill-top region [39, 40]. These chemical compositions are used as input to the OPAC model to obtained aerosol optical properties and compared with measured values. OPAC model is also used to distinguish the natural and anthropogenic aerosols by separating the natural and anthropogenic components. A scatter plot of monthly averaged AODs obtained from Microtops observations and OPAC model is shown in Figure 10. The solid line represents the 1:1 line. Model derived and observed AODs are linearly varying with a slope of 0.90 and very close to the 1:1 line which indicates that the model derived AOD are very close to the observed values. However, the model is underestimating the AOD by about 10%. This is due to the cut-off radius of aerosols at 7.5 micron considered by the model, but in reality, aerosols are larger, especially over semi-arid regions, though their residence period is only for a few hours and their contribution towards optical depth is small.

6.2. Source identification of natural and anthropogenic aerosols

Seven days air parcel back trajectories are considered to identify the possible source regions of the natural and anthropogenic aerosols at Mt. Abu. The back-trajectories during premonsoon and winter are shown in Figure 11(a) and (b), respectively. Air parcels are mainly coming from IGP during winter and the heights of the trajectories are within 2 km. Ground based observations show that BC values at Mt. Abu are higher during winter and it is also clearly seen that there is long-range transportation of anthropogenic aerosols like BC from IGP within the boundary layer height. On the other side, air parcels are direction during premonsoon season. The heights are also greater than 3 km. Earlier chemical analyses report that dust concentration during this season is maximum of about 80% (in mass) of the total aerosols [39]. Therefore, one can easily conclude by these trajectories that the source of these dust aerosols is the nearby desert region. The back-trajectory analysis indicates that there is significant contribution of IGP during winter enhancing anthropogenic aerosols and that by nearby arid region during premonsoon increasing natural dust aerosols.

7. Natural vs anthropogenic background aerosol radiative forcing

7.1. Seasonal variation of aerosol radiative forcing

Aerosol radiative forcing is estmated using SBDART model considering aerosol optical properties obtained from OPAC, aerosol vertical profile from CALIPSO and MODIS surface reflectance. Aerosol radiative forcings in different seasons are given in table 2. Aerosol radiative forcing is found to vary from -3.2 to +0.2 Wm^{-2} at TOA and from 6.1 to 23.6 Wm^{-2} within the atmosphere. Aerosol radiative forcing at TOA is found to be maximum of about $0.2\pm2.5\,Wm^{-2}$ during premonsoon, followed by -1.3$\pm$0.5, -2.7$\pm$1.6, and -3.1$\pm$1.3 Wm^{-2} during monsoon, winter and postmonsoon, respectively. Forcing within the atmosphere is maximum of about 23.6$\pm$5.5 Wm^{-2} during premonsoon, followed by 12.5$\pm$3.9, 7.4$\pm$1.8, and 6.1$\pm$1.8 Wm^{-2} during monsoon, postmonsoon and winter, respectively. Annual mean aerosol forcing at Mt. Abu is found to be 8.7$\pm$3.4 Wm^{-2} which is lower than other urban
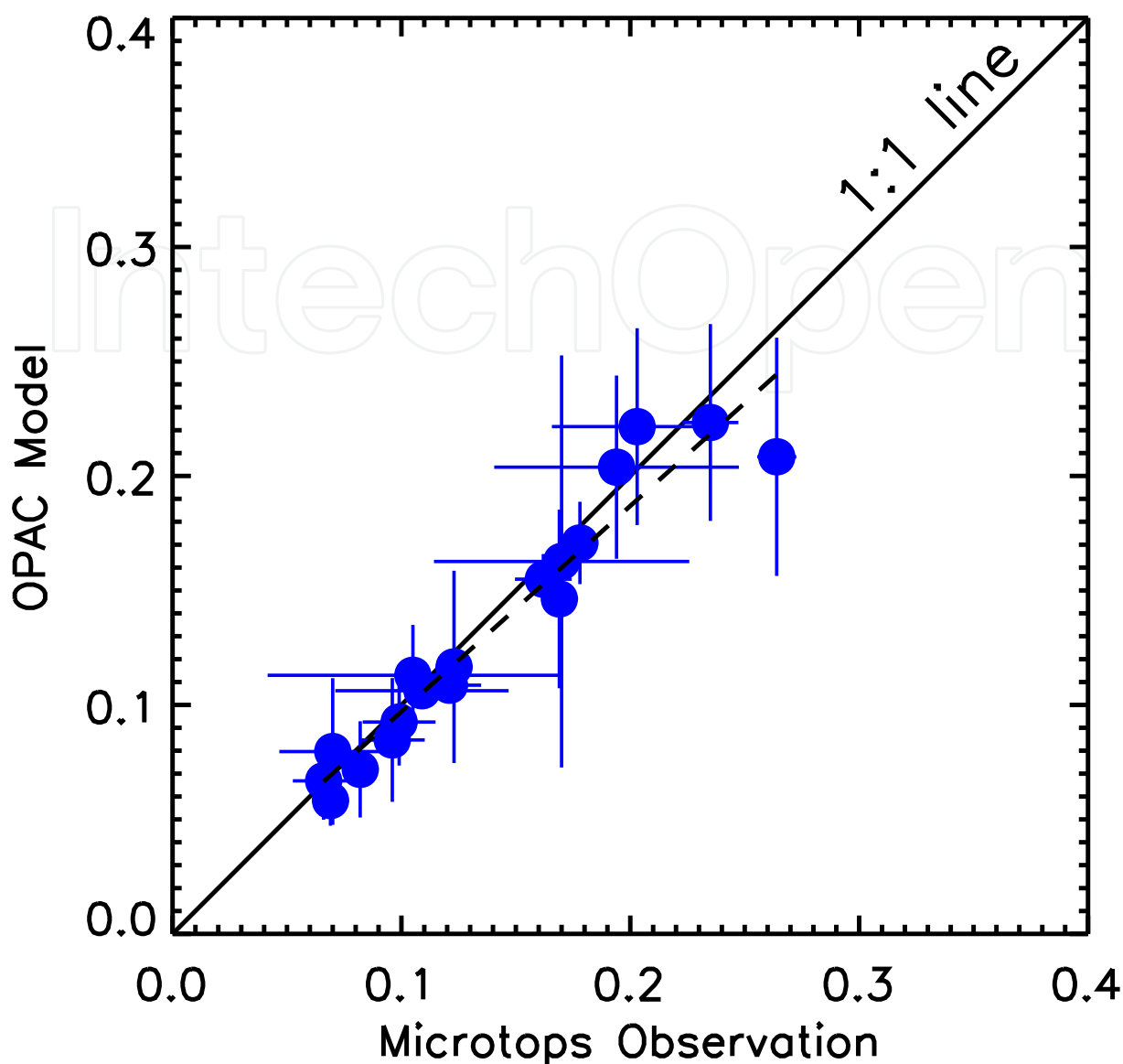
Figure 10. Scatter plot of monthly averaged AOD obtained from Microtops observations and OPAC model simulations. The solid line is the 1:1 line. The dashed line is the best-fitted line with a slope of 0.90, indicating that the OPAC underestimates AOD by 10%.

regions (mean forcing, 50 Wm^{-2}) and hill-top regions (mean forcing, 31 Wm^{-2}) in the Indian subcontinent [14]. For example, aerosol forcing over other hill-top regions like Pune, Kathmandu, Dibrugarh are about 33, 25 and 35.7 Wm^{-2}, respectively. These hilly areas are mainly influenced by anthropogenic aerosols. However, maximum forcing over Mt. Abu is found of about 23.6 Wm^{-2} during premonsoon which is lower but comparable with their forcing values. This is due to the maximum natural dust loading in the atmosphere at Mt. Abu.

Aerosol radiative forcing mainly depends on the amount of aerosol loading and underlying surface. Also, the sign of forcing at TOA is influenced by the aerosol type. An increase of absorbing aerosol loading causes positive forcing at TOA. In addition, bright surface which
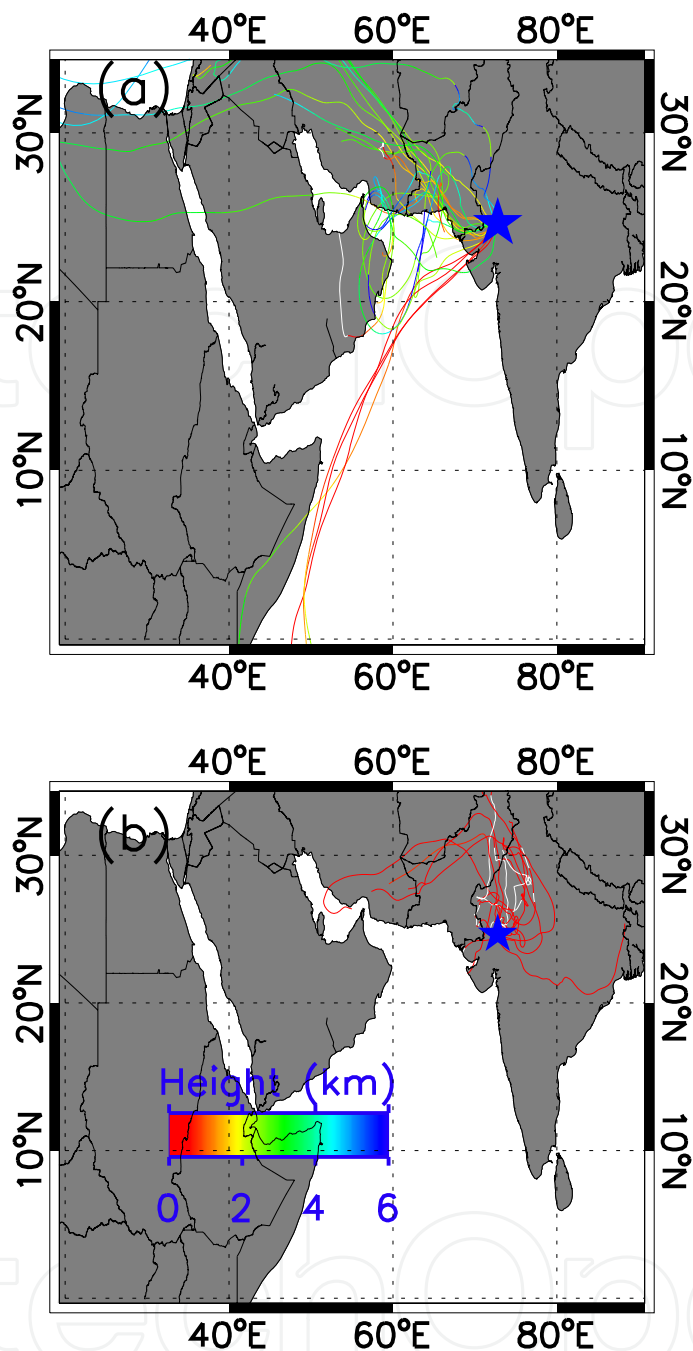
Figure 11. Seven days back trajectory analysis of aerosol parcels coming to Mt. Abu (location indicated by star) during (a) premonsoon and (b) winter. The color bar represents the height of the air parcels during their travel from source regions to the measurement site. Aerosols are mainly coming from desert region at higher altitude during premonsoon and from IGP within the boundary layer height (2 km) during winter.

reflects more solar radiation back to the space can cause positive TOA forcing. Radiative forcing at TOA changes its sign from negative to positive during premonsoon. This could be due to the combined effects of the relatively brighter land surface over western India and high dust loading in the atmosphere by frequently occurring dust storms over Thar Desert. TOA forcing becomes minimum during postmonsoon as land surface becomes darker by

Season	Aerosol Radiative		Forcing
	TOA	Surface	Atmosphere
Winter	-2.7	-8.8	6.1
Premonsoon	0.2	-23.4	23.6
Monsoon	-1.3	-13.8	12.5
Postmonsoon	-3.2	-10.6	7.4

Table 2. Seasonal variation of aerosol radiative forcing over Mt. Abu

the growing forest area over western India after monsoonal rain. Atmospheric forcing is proportionally varying with amount of aerosol loading. Maximum atmospheric forcing is found during premonsoon due to the maximum dust loading in this season while minimum forcing is observed during winter since the boundary layer height becomes lower than observational site which makes the site a free tropospheric station over western India with minimum aerosol loading in the atmosphere. During monsoon, heavy rains wash out the aerosols from the atmosphere, though atmospheric forcing is observed to be significantly high. This is due to the existence of aerosol layer, as found in the CALIPSO observations, that consist of large abundance of seasalt aerosols transported from Arabian Sea. This layer reflects the solar radiation significantly to the space which also causes relatively positive TOA forcing than that during winter and postmonsoon.

7.2. Contribution of natural and anthropogenic aerosols

Mt. Abu experiences large variation in aerosol properties and hence in the radiation forcing. During premonsoon there is large transportation of natural dust aerosols from surrounding arid region by the strong westerly wind and during monsoon large amount of seasalt is transported from the Arabian sea by the southwesterly wind. Figure 12 shows the seasonal variation of contributions of natural and anthropogenic forcings to the total aerosol radiative forcing within the atmosphere over Mt. Abu. The contributions of anthropogenic radiative forcing are 52%, 40%, 33%, and 56% and those of natural forcing are 48%, 60%, 67%, and 44% during winter, premonsoon, monsoon, and postmonsoon, respectively. Natural forcing is dominating at Mt. Abu during premonsoon and monsoon, whereas, the contributions of anthropogenic and natural forcing during winter and postmonsoon are almost equal. It is to be noted that natural and anthropogenic aerosol radiative forcings are calculated on the basis of their optical properties derived from OPAC model and OPAC model considers 7.5 μm as the upper limit of aerosol radius. In the present study dust is considered as natural aerosols, which in reality can be larger than this cut off limit over arid region, especially during premonsoon. Therefore, the contribution of natural forcing could be underestimated due to these large dust aerosols even though their AOD is very low. The comparison between OPAC and Microtops AOD indicates that this underestimation is not more that 10% (Figure 10).

Due to the proximity of Mt. Abu to the Thar desert dust aerosols are transported to this hill-top region during premonsoon and hence natural forcing is higher. During monsoon also, natural forcing is higher due to the large amount of seasalt coming from over the Arabian sea and simultaneously, dust and boundary layer anthropogenic aerosols are washed out by the heavy rains. Chemical analysis also shows that during monsoon, anthropogenic compositions like non-seasalt potassium, ammonium and nitrate are relatively less and the natural compositions like seasalt are enhanced over Mt. Abu [40, 63]. During postmonsoon, there is less transportation of seasalt aerosols to the measurement site due to low wind speed
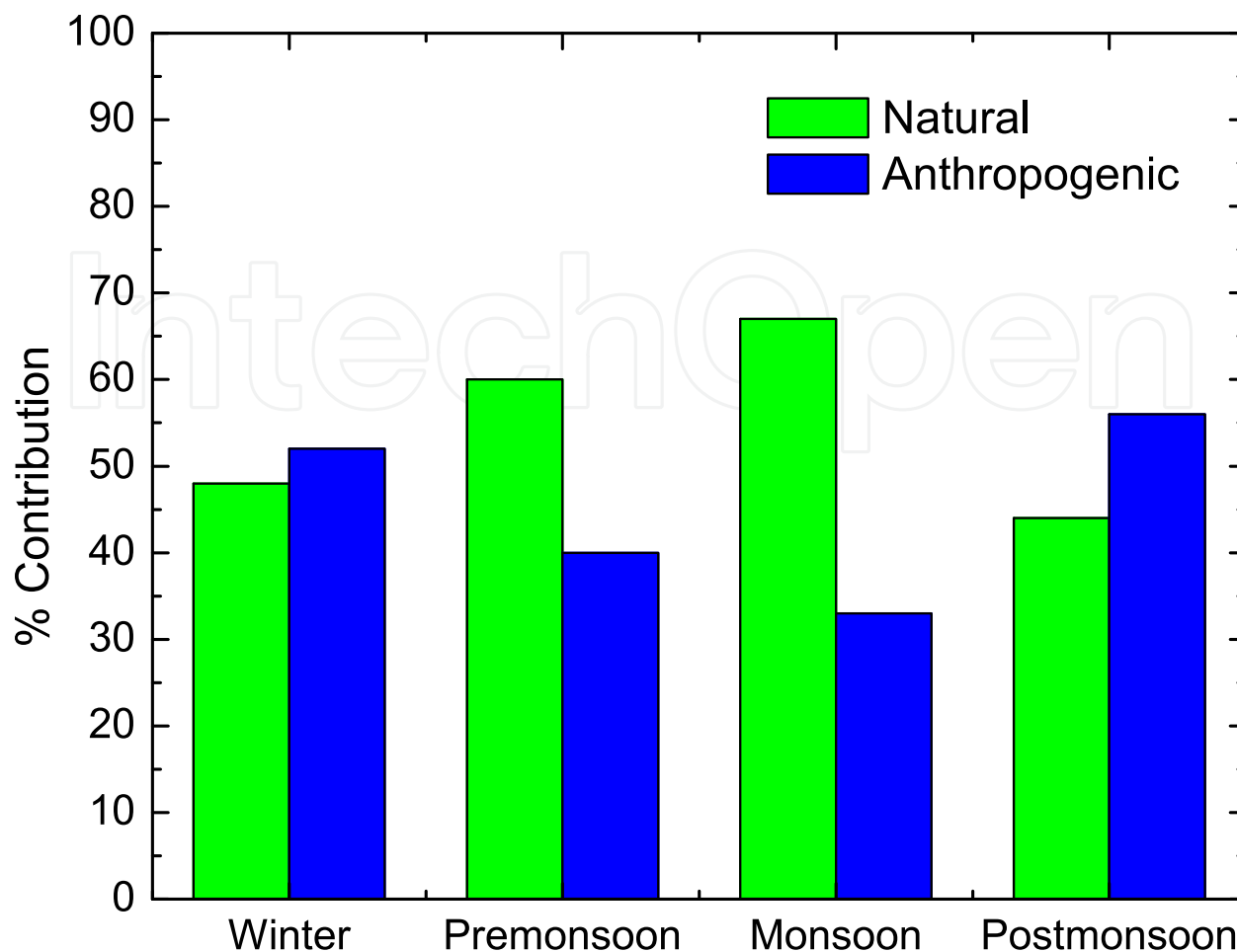
Figure 12. Seasonal variation of the contribution of natural and anthropogenic forcing to the total atmospheric radiative forcing over Mt. Abu.

and hence the natural forcing reduces and anthropogenic forcing increases. During winter, total aerosol loading is minimum as the measurement site becomes a free tropospheric station and thereby, both natural and anthropogenic forcings contribute equally.

Annual mean contributions of natural and anthropogenic forcing are about 55% and 45%, respectively. This indicates that anthropogenic aerosols are also significantly contributing to total radiative forcing within the atmosphere. This could be due to the close proximity of IGP which is a potential source of anthropogenic aerosols over semi-arid region. Therefore, it is concluded that western India is influenced by natural as well as anthropogenic aerosols significantly.

8. Conclusions

Western India is known for the presence of Thar Desert, which is a potential source of dust aerosols in the Indian subcontinent. Therefore, it is commonly believed that the atmosphere over western India is largely influenced by natural dust aerosols. With this motivation, the present study investigates the natural and anthropogenic contribution to the background aerosols and their radiative effects over western India. The optical and physical properties of aerosols over Mt. Abu, highest peak of the Aravalli mountains in western India are obtained

from a variety of ground-based and satellite-borne instruments. Mt. Abu is situated in the semi-arid region of Thar Desert and is less influenced by the local anthropogenic aerosols. It is therefore, a unique site for the observation of background aerosols over semi-arid region. Also, the Aravalli mountains are located in between Thar Desert and IGP which has large abundance of anthropogenic aerosols. Therefore, there is a significant variation of aerosol properties over Mt. Abu during different seasons, namely, winter (DJF), premonsoon (MAM), monsoon (JJA) and postmonsoon (SON). Ground-based observations show that AOD is maximum during premonsoon due to the large dust loading in the atmosphere by frequently occurring dust storms over Thar desert and minimum during winter due to low boundary layer height. Space-borne observations suggest that natural dust aerosols are dominating during premonsoon while anthropogenic aerosols are dominating during winter over western India. An interesting observation of CALIPSO is a layer of transported seasalt aerosols during monsoon over western India coming from Arabian Sea. These aerosols increase the contribution of natural forcing to the total atmospheric radiative forcing. Atmospheric radiative forcing is found to be maximum of about 23.6 ± 5.5 Wm^{-2} during premonsoon and minimum of about 6.1 ± 1.8 Wm^{-2} during winter. Another interesting result is TOA forcing is positive due to the bright land surface over western India during premonsoon, while it is negative during other seasons. The contribution of natural aerosols is found to be higher during premonsoon and monsoon and that of anthropogenic aerosols is higher during postmonsoon. During winter, they contribute equally. The annual average of natural and anthropogenic contribution is about 55% and 45%, respectively, indicating that the anthropogenic effects are also very significant. Thus the background aerosols over western India are not only influenced by desert dust aerosols but also by seasalt coming from Arabian Sea and anthropogenic aerosols transported from IGP.

Acknowledgment

Author details

Sanat Kumar Das
Department of Atmospheric Sciences, National Taiwan University, Taiwan

9. References

[1] Ackerman, A. S., Toon, O. B., Stevens, D. E., Heymsfield, A. J., Ramanathan, V. & Welton, E. J. [2000]. Reduction of tropical cloudiness by soot, *Science* 288: 1042–1047.

[2] Allen, A. G., Joy, L. & Petros, K. [1998]. Field validation of a semi-continuous method for aerosol black carbon (Aethalometer) and temporal patterns of summertime hourly black carbon measurements in southwestern PA, *Harvard School of Public Health*.

[3] Andreae, M. O. [1995]. *Climate effect of changing atmospheric aerosol levels, in Future Climates of the World, vol. 16 of World Survey of Climatology*, A. Henderson-Sellers, Ed. (Elsevier, Amsterdam).

[4] Badarinath, K. V. S., Kharol, S. K., Kaskaoutis, D. G., Sharma, A. R., Ramaswamy, V. & Kambezidis, H. D. [2010]. Long-range transport of dust aerosols over the Arabian Sea and Indian region – A case study using satellite data and ground-based measurements, *Global and Planetary Change* 72(3): 164–181.

[5] Bodhaine, B. A. [1995]. Aerosol absorption measurements at Barrow and Mauna Loa and the South Pole, *J. Geophy. Res.* 100: 8967– 8975.

[6] Bond, T. C., Bhardwaj, E., Dong, R., Jogani, R., Jung, S., Roden, C., Streets, D. G. & Trautmann, N. M. [2007]. Historical emissions of black and organic carbon aerosol from energy-related combustion, 1850–2000, *Global Biogeochemi. Cy.* 21(2): GB2018.

[7] Chand, D., Anderson, T. L., Wood, R., Charlson, R. J., Hu, Y., Liu, Z. & Vaughan, M. [2008]. Quantifying above-cloud aerosol using space borne lidar for improved understanding of cloudy-sky direct climate forcing, *J. Geophys. Res.* 113: 1–12.

[8] Chand, D., Wood, R., Anderson, T. L., Satheesh, S. K. & Charlson, R. J. [2009]. Satellite derived direct radiative effect of aerosols dependent on cloud cover, *Nature Geosc.* .

[9] Chiapello, I., Goloub, P., Tanre, D., Marchand, M., Hermann, J. & Torres, O. [2000]. Aerosol detection by TOMS and POLDER over oceanic region, *J. Geophy. Res.* 105: 7133–7142.

[10] Chýlek, P. & Coakley, J. A. [1974]. Aerosol and climate, *Science* 183: 75–77.

[11] Chýlek, P., Lohmann, U., Dubey, M., Mishchenko, M., Kahn, R. & Ohmura, A. [2007]. Limits on climate sensitivity derived from recent satellite and surface observations, *J. Geophys. Res.* 112.

[12] Chýlek, P., Ramaswamy, V. & Srivastava, V. [1984]. Graphitic carbon content of aerosols, clouds and snow and its climatic implications, *Sci. Total Environ.* 36: 117–120.

[13] d'Almeida, G. A., Koepke, P. & Shettle, E. P. [1991]. *Atmospheric Aerosols: Global Climatology and Radiative Characteristics*, A. Deepak, Hampton, Va.

[14] Das, S. K. & Jayaraman, A. [2011]. Role of black carbon in aerosol properties and radiative forcing over western india during premonsoon period, *Atmos. Res.* 102(3): 320–334.

[15] Das, S. K., Jayaraman, A. & Misra, A. [2008]. Fog-induced variations in aerosol optical and physical properties over the indo-gangetic basin and impact to aerosol radiative forcing, *Ann. Geophys.* 26: 1345–1354.

[16] Deepshikha, S., Satheesh, S. K. & Srinivasan, J. [2005]. Regional distribution of absorbing efficiency of dust aerosols over India and adjacent continents inferred using satellite remote sensing, *Geophys. Res. Lett.* 32.

[17] Dey, S., Tripathi, S. N., Singh, R. P. & Holben, B. N. [2004]. Influence of dust storms on the aerosol optical properties over the Indo-Gangetic basin, *J. Geophy. Res.* 109.

[18] Ganguly, D. & Jayaraman, A. [2006]. Physical and optical properties of aerosols over an urban location in western India: Implications for shortwave radiative forcing, *J. Geophy. Res.* 111: 1–13.

[19] Ganguly, D., Jayaraman, A. & Gadhavi, H. [2006]. Physical and optical properties of aerosols over an urban location in western India: Seasonal variabilities, *J. Geophy. Res.* 111.

[20] Gao, B.-C., Kaufman, Y. J., Tanre, D. & Li, R.-R. [2002].   Distinguishing tropospheric aerosols from thin cirrus clouds for improved aerosol retrievals using the ratio of 1.38-μm and 1.24-μm channels, *Geophys. Res. Lett.* 29(18): 1890.

[21] Hansen, A. D. A., Rosen, H. & Novakov, T. [1982].   Real-time measurement of the absorption coefficient of aerosol particles, *Appl. Opt.* 21: 3060–3062.

[22] Hansen, J. E. [1969]. Exact and approximate solutions for multiple scattering by cloudy and hazy planetary atmospheres, *J. Atmos. Sci.* 26: 478–487.

[23] Haywood, J. M. & Ramaswamy, V. [1998]. Global sensitivity studies of the direct radiative forcing due to anthropogenic sulfate and black carbon aerosols, *J. Geophy. Res.* 103 (D3): 6043–6058.

[24] Haywood, J. M. & Shine, K. P. [1995]. The effect of anthropogenic sulfate and soot aerosol on the clear sky planetary radiation budget, *Geophys. Res. Lett.* 22: 603–606.

[25] Herman, J. R., Bhartia, P. K., Torres, O., Hsu, N. C., Seftor, C. J. & Celarier, E. [1997]. Global distribution of uv-absorbing aerosols from Nimbus-7/TOMS data, *J. Geophy. Res.* 102: 16,911–16,922.

[26] Hess, M., Keopke, P. & Schult, I. [1998]. Optical properties of aerosols and clouds: The software package OPAC, *Bull. Am. Meteorol. Soc.* 79: 831–844.

[27] Houghton, J. T., Ding, Y., Griggs, D. J., Noguer, M., van der Linden, P. J. & Xiaosu, S. [2001]. *Climate Change 2001: The Scientific Basis*, Cambridge Univ. Press, New York.

[28] Hsu, N. C., Herman, J. R. & Weaver, C. [2000]. Determination of radiative forcing of Saharan dust using combined TOMS and ERBE data, *J. Geophy. Res.* 105: 20,649–20,661.

[29] Hsu, N. C., Tsay, S.-C., King, M. D. & Herman, J. R. [2004]. Aerosol properties over bright-reflecting source regions, *IEEE Trans, Geosci. Remote Sens.* 42(3): 557–569.

[30] Ichoku, C., Levy, R., Kaufman, Y. J., Remer, L. A., Li, R.-R., Martins, V. J., Holben, B. N., Abuhassan, N., Slutsker, I., Eck, T. F. & Pietras, C. [2002]. Analysis of the performance characteristics of the five-channel Microtops II sun photometer for measuring aerosol optical thickness and precipitable water vapor, *J. Geophy. Res.* 107 (D13): 417.

[31] Jacobson, M. Z. [2001]. Strong radiative heating due to the mixing state of black carbon in atmospheric aerosols, *Nature* 409: 695–697.

[32] Jayaraman, A., Gadhavi, H., Ganguly, D., Misra, A., Ramachandran, S. & Rajesh, T. A. [2006]. Spatial variations in aerosol characteristics and regional radiative forcing over India: Measurements and modeling of 2004 road campaign experiment, *Atmos. Environ.* 40: 6504–6515.

[33] Jayaraman, A., Lubin, D., Ramachandran, S., Ramanathan, V., Woodbridge, E., Collins, W. D. & Zalpuri, K. S. [1998]. Direct observation of aerosol radiative forcing over the tropical Indian Ocean during the January-February 1996 pre-INDOEX cruise., *J. Geophy. Res.* 103 (D12): 13827–13836.

[34] Kaufman, Y. J., Tanre, D., Holben, B. N., Mattoo, S., Remer, L. A., Eck, T. F., Vaughan, J. & Chatene, B. [2002]. Aerosol radiative impact on spectral solar flux at the surface, derived from principal-plane sky measurements, *J. Atmos. Sci.* 59: 635–646.

[35] Kaufman, Y. J., Tanré, D., Remer, L. A., Vermote, E. F., Chu, A. & Holben, B. N. [1997]. Operational remote sensing of tropospheric aerosol over land from EOS moderate resolution imaging spectroradiometer, *J. Geophy. Res.* 102(D14): 17,051–17,067.

[36] Kondratyev, K. Y. [1969]. *Radiation in the Atmosphere*, Academic Press.

[37] Krishnan, P. & Kunhikrishnan, P. K. [2004]. Temporal variations of ventilation coefficient at a tropical indian station using uhf wind profiler, *Curr. Sci.* 86(3): 477–451.

[38] Krishnan, R. & Ramanathan, V. [2002]. Evidence of surface cooling from absorbing aerosols, *Geophys. Res. Lett.* 29(9): 1340.

[39] Kumar, A. & Sarin, M. M. [2009]. Mineral aerosols from western india: Temporal variability of coarse and fine atmospheric dust and elemental characteristics, *Atmos. Environ.* 43(26): 4005–4013.

[40] Kumar, A. & Sarin, M. M. [2010]. Atmospheric water-soluble constituents in fine and coarse mode aerosols from high-altitude site in western india: Long-range transport and seasonal variability, *Atmos. Environ.* 44(10): 1245–1254.

[41] Kumar, N., Chu, A. & Foster, A. [2007]. An empirical relationship between PM2.5 and aerosol optical depth in Delhi Metropolitan, *Atmos. Environ.* 41(21): 4492–4503.

[42] Lelieveld, J., Crutzen, P. J., Ramanathan, V., Andreae, M. O., Brenninkmeijer, C. A. M., Campos, T., Dickerson, G. R. C. R. R., de Gouw, H. F. J. A., Hansel, A., Jefferson, A., Kley, D., de Laat, A. T. J., Lal, S., Lawrence, M. G., Lobert, J. M., Mayol-Bracero, O. L., Mitra, A. P., Novakov, T., Oltmans, S. J., Prather, K. A., Reiner, T., Rodhe, H., Scheeren, H. A., Sikka, D. & Williams, J. [2002]. The Indian Ocean Experiment: Widespread Air Pollution from South and Southeast Asia, *Science* 291: 1031–1036.

[43] Levy, R. C., Remer, L. A., Mattoo, S., Vermote, E. F. & Kaufman, Y. J. [2007]. Second-generation operational algorithm: Retrieval of aerosol properties over land from inversion of moderate resolution imaging spectroradiometer spectral reflectance, *J. Geophys. Res.* 112(D13): D13211.

[44] Levy, R. C., Remer, L. A., Tanré, D., Kaufman, Y. J., Ichoku, C., Holben, B. N., Livingston, J. M., Russell, P. B. & Maring, H. [2003]. Evaluation of the Moderate-Resolution imaging spectroradiometer (MODIS) retrievals of dust aerosol over the ocean during PRIDE, *J. Geophy. Res.* 108(D19): 8594.

[45] Martins, J. V., Tanré, D., Remer, L., Kaufman, Y., Mattoo, S. & Levy, R. [2002]. MODIS cloud screening for remote sensing of aerosols over oceans using spatial variability, *Geophys. Res. Lett.* 29(12): 8009.

[46] Menon, S., Hansen, J., Nazarenko, L. & Luo, Y. [2002]. Climate effects of black carbon aerosols in China and India, *Science* 297: 2250–2253.

[47] Mishchenko, M. I., Geogdzhayev, I. V., Rossow, W. B., Cairns, B., Carlson, B. E., Lacis, A. A., Liu, L. & Travis, L. D. [2007]. Long-term satellite record reveals likely recent aerosol trend, *Sscience* 315: 1543.

[48] Moorthy, K. K., Satheesh, S. K., Babu, S. S. & Dutt, C. B. S. [2008]. Integrated Campaign for Aerosols, gases and Radiation Budget (ICARB): An overview, *J. of Earth System Sci.* 117: 243–262.

[49] Morys, M., Mims, F. M., Hagerup, S., Anderson, S. E., Baker, A., Kia, J. & Walkup, T. [2001]. Design and calibration and performance of MICROTOPS II handheld ozone monitor and Sun photometer, *J. Geophy. Res.* 106 (D3): 14,573–14,582.

[50] Nair, V. S., Moorthy, K. K., Denny, A. P., Kunhikrishnan, P. K., George, S., Nair, P. R., Babu, S. S., Abish, B., Satheesh, S. K., Tripathi, S. N., Niranjan, K., Madhavan, B. L., Srikant, V., Dutt, C. B. S., Badarinath, K. V. S. & Reddy, R. R. [2007]. Wintertime aerosol characteristics over the Indo-Gangetic Plain (IGP): Impacts of local boundary layer processes and long-range transport, *J. Geophy. Res.* 112.

[51] Nakajima, T., Tanaka, M., Yamano, M., Shiobara, M., Arao, K. & Nakanishi, Y. [1989]. Aerosol optical characteristics in the yellow sand events observed in May, 1982 at Nagasaki, part 2, Models, *J. Meteorol. Soc. Jpn* 67: 279–291.

[52] Niranjan, K., Devi, T. A., Spandana, B., Sreekanth, V. & Madhavan, B. L. [2012]. Evidence for control of black carbon and sulfate relative mass concentrations on composite aerosol radiative forcing: Case of a coastal urban area, *J. Geophy. Res.* 117(D5).

[53] Novakov, T., Andreae, M. O., Gabriel, R., Kirchstetter, T. W., Mayol-Bracero, O. L. & Ramanathan, V. [2000]. Origin of carbonaceous aerosols over the tropical Indian Ocean: Biomass burning or fossil fue, *Geophys. Res. Lett.* 27(4): 4061–4064.

[54] Pandithurai, G., Dipu, S., Dani, K. K., Tiwari, S., Bisht, D. S., Devara, P. C. S. & Pinker, R. T. [2008]. Aerosol radiative forcing during dust events over New Delhi, India, *J. Geophy. Res.* 113.

[55] Pant, P., Hegde, P., Dumka, U. C., Sagar, R., Satheesh, S. K., Moorthy, K. K., Saha, A. & Srivastava, M. K. [2006]. Aerosol characteristics at a high-altitude location in central Himalayas: Optical properties and radiative forcing, *J. Geophy. Res.* 111.

[56] Pierluissi, J. H. & Peng, G. S. [1985]. New molecular transmission band models for LOWTRAN, *Opt. Eng.* 24(3): 541–547.

[57] Quinn, P. K. & Bates, T. S. [2005]. Regional aerosol properties: Comparisons of boundary layer measurements from ACE 1, ACE 2, Aerosols99, INDOEX, ACE Asia, TARFOX, and NEAQS, *J. Geophys. Res.* 110.

[58] Quinn, P. K., Bates, T. S., Coffman, D. J., Miller, T. L., Johnson, J. E., Covert, D. S., Putaud, J. P., Neususs, C. & Novakov, T. [2000]. A comparison of aerosol chemical and optical properties from the 1st and 2nd Aerosol Characterization Experiments, *Tellus, Ser. B* 52: 239–257.

[59] Ramachandran, S., Rengarajan, R., Jayaraman, A., Sarin, M. M. & Das, S. K. [2006]. Aerosol radiative forcing during clear, hazy, and foggy conditions over a continental polluted location in north India, *J. Geophy. Res.* 111.

[60] Ramanathan, V., Chung, C., Kim, D., Bettge, T., Buja, L., Kiehl, J. T., Washington, W. M., Fu, Q., Sikka, D. R. & Wild, M. [2005]. Atmospheric brown clouds: Impacts on South Asian climate and hydrological cycle, *PNAS* 102 (4): 5326–5333.

[61] Ramanathan, V., Crutzen, P. J., Lelieveld, J., Mitra, A. P., Althausen, D., Anderson, J., Andreae, M. O., Cantrell, W., Cass, G. R., Chung, C. E., Clarke, A. D., Coakley, J. A., Collins, W. D., Conant, W. C., Dulac, F., Heintzenberg, J., Heymsfield, A. J., Holben, B., Howell, S., Hudson, J., Jayaraman, A., Kiehl, J. T., Krishnamurti, T. N., Lubin, D., McFarquhar, G., Novakov, T., Ogren, J. A., Podgorny, I. A., Prather, K., Priestley, K., Prospero, J. M., Quinn, P. K., Rajeev, K., Rasch, P., Rupert, S., Sadourny, R., Satheesh, S. K., Shaw, G. E., Sheridan, P. & Valero, F. P. J. [2001]. Indian ocean experiment: An integrated analysis of the climate forcing and effects of the great Indo-Asian haze, *J. Geophy. Res.* 106: 28,371–28,398.

[62] Ramanathan, V., Ramana, M. V., Roberts, G., Kim, D., Corrigan, C., Chung, C. & Winker, D. [2007]. Warming trends in Asia amplified by brown cloud solar absorption, *Nature* 448: 575–578.

[63] Rastogi, N. & Sarin, M. M. [2005a]. Chemical characteristics of individual rain events from a semi-arid region in India: Three-year study, *Atmos. Environ.* 39: 3313–3323.

[64] Rastogi, N. & Sarin, M. M. [2005b]. Long-term characterization of ionic species in aerosols from urban and high-altitude sites in western India: Role of mineral dust and anthropogenic sources, *Atmos. Environ.* 39: 5541–5554.

[65] Reeves, R. G., Anson, A. & Eds, D. L. [1975]. *Manual of Remote Sensing*, Amer. Soc. Photogrammetry.

[66] Reid, J. S., Eck, T. F., Christopher, S. A., Hobbs, P. V. & Holben, B. N. [1999]. Use of the Ångström exponent to estimate the variability of optical and physical properties of aging smoke particles in brazil and, *J. Geophy. Res.* 104: 473–489.

[67] Remer, L. A., Kaufman, Y. J., Tanre, D., Mattoo, S., Chu, D. A., Martins, J. V., Li, R.-R., Choku, C., Levy, R. C., Kleidman, R. G., Eck, T. F., Vermote, E. & Holben, B. N. [2005]. The MODIS aerosol algorithm, products and validation, *J. Atmos. Sci.* 62: 947–973.

[68] Ricchiazzi, P., Yang, S., Gautier, C. & Sowle, D. [1998]. SBDART, A research and teaching tool for plane-parallel radiative transfer in the Earth's atmosphere, *Bull. Am. Meteorol. Soc.* 79: 2101–2114.

[69] Saha, A. & Krishna Moorthy, K. [2004]. Impact of precipitation on aerosol spectral optical depth and retrieved size distributions: A case study, *J. Appl. Meteor.* 43(6): 902–914.

[70] Satheesh, S. K. & Ramanathan, V. [2000]. Large differences in tropical aerosol forcing at the top of the atmosphere and Earth's surface, *Nature* 405: 60–63.

[71] Satheesh, S. K. & Srinivasan, J. [2002]. Enhanced aerosol loading over Arabian Sea during the pre-monsoon season: Natural or anthropogenic?, *Geophys. Res. Lett.* 29(18): 1874.

[72] Shettle, E. P. & Fenn, R. W. [1975]. Models of the atmospheric aerosols and their optical properties., *AGARD Conf. Proc., Optical Propagation in the Atmosphere, Lyngby, Denmark, NATO Advisory Group for Aerospace Research* pp. 2.1–2.16.

[73] Staetter, R. & Schroeder, M. [1978]. Spectral characteristics of natural surfaces, *Proc. Int. Conf. on Earth Observation from Space and Management of Planetary Resources, Toulouse, France, Council of Europe, Commission of the European Communities, and European Association of Remote Sensing Laboratories,* p. 661.

[74] Stamnes, K., Tsay, S., Wiscombe, W. & Jayaweera, K. [1988]. Numerically stable algorithm for discrete-ordinate-method radiative transfer in multiple scattering and emitting layered media, *Appl. Opt.* 27: 2502–2509.

[75] Subbaraya, B. H., Jayaraman, A., Krishnamoorthy, K. & Mohan, M. [2000]. Atmospheric aerosol studies under isroâĂŹs geosphere biosphere programs, *J. Ind. Geophys. Union* 4: 77–90.

[76] Tanre, D., Deroo, C., Duhaut, P., Herman, M., Morcrette, J. J., Perbos, J. & Deschamps, P. Y. [1990]. Description of a computer code to simulate the satellite signal in the solar spectrum: The 5S code, *Int. J. Remote Sens.* 11(4): 659–668.

[77] Tanré, D., Deschamps, P. & Herman, C. D. M. [1988]. Estimation of saharan aerosol optical thickness from blurring effects in thematic mapper data, *J. Geophy. Res.* 93(D12): 15955–15964.

[78] Tanré, D., Haywood, J., Pelon, J., FLeón, J., Chatenet, B., Formenti, P., Francis, P., Goloub, P., Highwood, E. J. & Myhre, G. [2003]. Measurement and modeling of the saharan dust radiative impact: Overview of the Saharan Dust Experiment (SHADE), *J. Geophy. Res.* 108(D18): 8574.

[79] Tanré, D., Herman, M. & Kaufman, Y. J. [1996]. Information on aerosol size distribution contained in solar reflected spectral radiances, *J. Geophy. Res.* 101(D14): 19,042–19,060.

[80] Tanré, D., Kaufman, Y. J., Herman, M. & Mattoo, S. [1997]. Remote sensing of aerosol properties over oceans using the MODIS/EOS spectral radiances, *J. Geophys. Res.* 102(D14): 16,971–16,988.

[81] Tomasi, C., Caroli, E. & Titale, V. [1983]. Study of the relationship between Ångström's wavelength exponent and junge particle size distribution exponent, *J. Clim. Appl. Meteorol.* 22: 1707–1716.

[82] Torres, O., Bhartia, P. K., Herman, J. R., Ahmad, Z. & Gleason, J. [1998]. Derivation of aerosol properties from satellite measurements of backscattered ultraviolet radiation, Theoretical basis, *J. Geophy. Res.* 103: 17,099 –17,110.

[83] Tsai, T.-C., Jeng, Y.-J., Chu, D. A., Chen, J.-P. & Chang, S.-C. [2011]. Analysis of the relationship between MODIS aerosol optical depth and particulate matter from 2006 to 2008, *Atmos. Environ.* 45(27): 4777–4788.

[84] van de Hulst, H. C. [1968]. Asymptotic fitting, a method for solving anisotropic transfer problems in thick layers, *J. Comput. Phys.* 3: 291–306.

[85] Vaughan, M. A., Winker, D. M. & Powell, K. A. [2005]. CALIOP algorithm theoretical basis document, part 2: Feature detection and layer properties algorithms,Rep.PC-SCI-202, *NASA Langley Res. Cent., Hampton, Va* pp. 1–87.

[86] Venkataraman, C., Habib, G., Eiguren-Fernandez, A., Miguel, A. H. & Friedlander, S. K. [2005]. Residential biofuels in South Asia:carbonaceous aerosol emissions and climate impacts, *Science* 307: 1454–1456.

[87] Vernier, J. P., Pommereau, J. P., Garnier, A., Pelon, J., Larsen, N., Nielsen, J., Christensen, T., Cairo, F., Thomason, L. W., Leblanc, T. & McDermid, I. S. [2009]. Tropical stratospheric aerosol layer from calipso lidar observations, *J. Geophys. Res.* 114.

[88] Weare, B., Temkin, R. & Snell, F. [1974]. Aerosols and Climate: Some further considerations, *Science* 186: 827–828.

[89] Weingartner, E., Saathoff, H., Schnaiter, M., Streit, N., Bitnar, B. & Baltensperger, U. [2003]. Absorption of light by soot particles: Determination of the absorption coefficient by means of aethalometers, *J. Aerosol Sci.* 34: 1445–1463.

[90] Wielicki, B. A., Wong, T., Allan, R. P., Slingo, A., Kiehl, J. T., Soden, B. J., Gordon, C. T., Miller, A. J., Yang, S.-K., Randall, D. A., Robertson, F., Susskind, J. & Jacobowitz, H. [2002]. Evidence for large decadal variability in the tropical mean radiative energy budget, *Science* 295: 841–844.

[91] Wiscombe, W. J. & Warren, S. G. [1980]. A model for the spectral albedo of snow. Part I: Pure snow, *J. Atmos. Sci.* 37: 2712–2733.

[92] Yadav, S. & Rajamani, V. [2004]. Geochemistry of aerosols of northwestern part of India adjoining the Thar Desert, *Geochim. Cosmochim. Ac.* 68: 1975–1988.